

# First-principles study of $\text{InVO}_4$ under pressure: phase transitions from $\text{CrVO}_4$ - to $\text{AgMnO}_4$ -type structure

Sinhué López-Moreno<sup>1,\*†</sup>, Plácida Rodríguez-Hernández<sup>3,‡</sup>, Alfonso Muñoz<sup>3,‡</sup>  
and Daniel Errandonea<sup>2¶</sup>

<sup>†1</sup>*CONACYT - Centro de Investigación en Corrosión, Universidad Autónoma de Campeche, Av. Héroe de Nacozari 480, Campeche, Campeche 24029, México*

<sup>‡3</sup>*MALTA Consolider Team, Departamento de Física, Instituto de Materiales y Nanotecnología, and Malta Consolider Team, Universidad de La Laguna, La Laguna 38205, Tenerife*

<sup>¶2</sup>*MALTA Consolider Team, Departamento de Física Aplicada-ICMUV, Universidad de Valencia, Edificio de Investigación, c/Dr. Moliner 50, Burjassot, 46100 Valencia, Spain*

E-mail: sinlopez@uacam.mx

## Abstract

First-principles calculations have been done to study the  $\text{InVO}_4$  compound under pressure. In this work, total energy calculations were performed in order to analyze the structural behavior of the experimentally known polymorphs of  $\text{InVO}_4$ :  $\alpha$ - $\text{MnMoO}_4$ -type (I),  $\text{CrVO}_4$ -type (III), and the wolframite (V). Besides, in this paper we present our results about the stability of this compound beyond the pressures reached by experiments. We propose some new high pressure phases based in the study of 13 possible candidates. The quasiharmonic approximation has been used to calculate the sequence of phase transitions at 300 K:  $\text{CrVO}_4$ -type, III (in parentheses the transition pressure)  $\rightarrow$  wolframite, V (4.4 GPa)  $\rightarrow$  raspite, VI (28.1 GPa)  $\rightarrow$   $\text{AgMnO}_4$ -type, VII (44 GPa). Equations of state and phonon frequencies as function of pressure have been calculated for the studied phases. In order to determine the stability of each phase we also report the phonon dispersion along the Brillouin zone and the phonon density of states for the most stable polymorphs. Finally, the electronic band structure for the low- and high-pressure phases for the studied polymorphs is presented as well as the pressure evolution of the band gap by using the HSE06 hybrid functional.

## 1 Introduction

Vanadates  $\text{AVO}_4$ <sup>1</sup> oxides have been the focus of many studies due to their wide physical properties which leads to important applications in various fields, such as thermophosphorus sensors, high-power lasers, scintillators, active material for gas sensors, catalysis for water splitting and electrolyte for lithium ion batteries, to name a few.<sup>1-10</sup> Several vanadates can crystallize in structures such as zircon [space group (SG):  $I4_1/amd$ , No. 141,  $Z = 4$ , crystal structure (CS): tetragonal],<sup>11,12</sup> scheelite (SG:  $I4_1/a$ , No. 88,  $Z = 4$ , CS: tetragonal),<sup>13</sup> and monazite (SG:  $P2_1/n$ , No. 14,  $Z = 4$ , CS: monoclinic),<sup>14</sup> however, to our knowledge, only the vanadates  $\text{CrVO}_4$ -III,  $\text{FeVO}_4$ -II,  $\text{TlVO}_4$  and  $\text{InVO}_4$ , have been synthesized in the  $\text{CrVO}_4$ -type structure (SG:  $Cmcm$ , No. 63,  $Z = 4$ , CS: orthorhombic).<sup>6</sup> While  $\text{CrVO}_4$ -III and  $\text{FeVO}_4$ -II

have been studied by using several techniques,<sup>15–19</sup> only the thermodynamic properties,<sup>20</sup> the vibrational spectra,<sup>21</sup> and the photoelectrochemical response<sup>9</sup> were reported for  $\text{TlVO}_4$ . In contrast, there have been more studies dedicated to study  $\text{InVO}_4$  due to its potential for applications such as a catalyst for production of hydrogen by visible-light driven water splitting.<sup>7–10,22,23</sup>

$\text{InVO}_4$  can be synthesized in different polymorphic forms depending on the preparation and temperature conditions:  $\text{InVO}_4$ -I which has the  $\alpha$ - $\text{MnMoO}_4$ -type structure (SG:  $C2/m$ , No. 12,  $Z = 8$ , CS: monoclinic),  $\text{InVO}_4$ -II (undetermined structure), and the  $\text{InVO}_4$ -III also identified as the  $\text{CrVO}_4$ -type structure.<sup>20,24–29</sup> Besides, two high pressure (HP) phases have been reported:  $\text{InVO}_4$ -IV (undetermined structure) and  $\text{InVO}_4$ -V<sup>25</sup> that has the characteristic wolframite structure of several  $\text{AWO}_4$  compounds (SG:  $P2/c$ , No. 13,  $Z = 2$ , CS: monoclinic).<sup>30</sup> The high pressure phenomena and the studies of phase transitions driven by pressure in  $\text{ABO}_4$  compounds are broadly reviewed in Refs. 1, 31 and 32, to name a few. Figure 1 (a)-(c) shows the crystal structure of these phases, with the coordination polyhedra of In and V depicted in each figure. The most representative works on this compound have been dedicated to describe the crystalline structure of the phases III and V, whereas there is a latent lack of information regarding phases I, II, and IV, due to their relative stability against to the others.

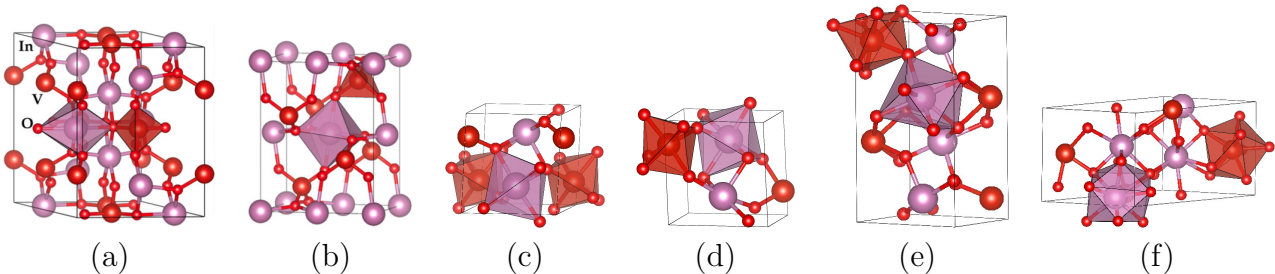


Figure 1: (Color online) Most relevant crystalline structures of  $\text{InVO}_4$  polymorphs: (a)  $\alpha$ - $\text{MnMoO}_4$ -type, (b)  $\text{CrVO}_4$ -type, (c) wolframite, (d)  $\text{CuWO}_4$ -type, (e) raspite, and (f)  $\text{AgMnO}_4$ -type.

Regarding phase V, the wolframite structure matches with the high pressure phase reported for other compounds with  $\text{CrVO}_4$ -type structure such as  $\text{InPO}_4$  and  $\text{TiPO}_4$ .<sup>33</sup> Besides,

this phase is considered as a natural high-pressure post-CrVO<sub>4</sub>-type structure in the phase diagram proposed for these kind of compounds.<sup>6</sup> Although the study performed by Errandonea *et al.*<sup>25</sup> is a novelty and present important information about the stability of this compound under pressure, other transitions could be observed at higher pressures than those reached in their experiments. Moreover, it has been demonstrated that theoretical studies can provide new insights about the stability of ABX<sub>4</sub> compounds under pressure,<sup>1</sup> which could help to explore and understand the behavior of vanadates beyond the wolframite phase.

As well as studies on the crystalline CrVO<sub>4</sub>-type structure of InVO<sub>4</sub>, there have been investigations dedicated to the study of other forms of this compound. In these efforts, it was reported the synthesis and characterization of InVO<sub>4</sub> nanotubes arrays.<sup>34-36</sup> It is interesting to mention that these arrays can present either the  $\alpha$ -MnMoO<sub>4</sub>-type structure<sup>34,36</sup> or the orthorhombic CrVO<sub>4</sub>-type structure,<sup>36</sup> whereas nanoribbons synthesized by hydrothermal process present the orthorhombic one. On the other hand, it has been reported that nanofibers of InVO<sub>4</sub> can present both structures.<sup>37</sup> These results show the importance of studying the known polymorphs of InVO<sub>4</sub>.

In an effort to get a better understanding of the behavior of InVO<sub>4</sub> at equilibrium and under pressure, we carry out *ab initio* calculations by considering first the well known experimental synthesized phases of this compound to determine the stability of each reported structure: InVO<sub>4</sub>-I, -III, and -V phases were studied. A complete description of the stable phases is presented in conjunction with the experimental data from literature. After, we go further and we put forward other possible high pressure phases for a range of pressure beyond the one reached in the experiments performed by Errandonea *et al.*<sup>25</sup> to determine the transition pressures at ambient temperature and the range of pressure stability of each phase by using the quasiharmonic approximation. We also report the evolution of phonon frequencies for the most stable polymorphs as well as the phonon spectrum and phonon density of states (phonon DOS) of each phase, which in turns will help us to determine the stability of each phase. In an effort to complement our study, we performed the band

structure calculations for the most representative phases of  $\text{InVO}_4$ .

The paper is organized as follows: In the next section, we give a detailed description of the computational procedure. The description of the structure of the experimentally known polymorphs of  $\text{InVO}_4$  is presented in Sec. 3.1, while the phase transitions driven by pressure are on Sec. 3.2. The study of vibrational and electronic properties of  $\text{InVO}_4$  are shown in Sec. 3.3 and 3.4, respectively. Finally, the summary and conclusions are given in Sec. 4.

## 2 Computational details

Calculations of the total energy were performed within the framework of the density functional theory (DFT) and the projector-augmented wave (PAW)<sup>38,39</sup> method as implemented in the Vienna *ab initio* simulation package (VASP).<sup>40-43</sup> A plane-wave energy cutoff of 520 eV was used to ensure a high precision in our calculations. The exchange-correlation energy was described within the generalized gradient approximation (GGA) in the AM05<sup>44-46</sup> formulation.

The Monkhorst-Pack scheme was employed to discretize the Brillouin-zone (BZ) integrations<sup>47</sup> with meshes  $3\times 3\times 3$ ,  $4\times 3\times 3$ ,  $4\times 4\times 2$ ,  $4\times 4\times 4$ , and  $4\times 4\times 2$ , which correspond to sets of 10, 8, 4, 16, and 8, special  $k$ -points in the irreducible BZ for the  $\alpha$ - $\text{MnMoO}_4$ -type structure,  $\text{CrVO}_4$ -type structure, scheelite, wolframite, raspite (SG:  $P2_1/a$ , No. 14,  $Z=4$ , CS: monoclinic; this phase is the low temperature monoclinic dimorph of stolzite), and  $\text{AgMnO}_4$ -type structure (SG:  $P2_1/n$ , No. 14,  $Z = 4$ , CS: monoclinic), respectively. For the other phases considered in the high-pressure regime, we use the most suitable mesh for each case. In the relaxed equilibrium configuration, the forces are less than 2 meV/Å per atom in each of the Cartesian directions. This high degree of convergence is required for the calculations of vibrational properties using the direct force constant approach.<sup>48</sup> The phonon DOS, has been obtained from the calculation of the phonons in the whole BZ with a supercell  $2\times 2\times 2$  times the conventional unit cell by using the PHONON software.<sup>48</sup> The calculations

of phonon spectrum were done for several volume points: 8 (for a range of pressure from  $\approx 0$  to 7 GPa), 11 (from 3.6 to 35 GPa), 9 (from 22 to 51 GPa), and 6 (from 39.7 to 62 GPa) for the  $\text{CrVO}_4$ -type structure, wolframite, raspite, and the  $\text{AgMnO}_4$ -type structure, respectively. Temperature effects and zero-point energy have been included within the quasi-harmonic approximation<sup>49</sup> through the calculation of the vibrational free energy, the method is well explained on references 50 and 51. The phase transitions at 300 K were obtained analyzing the Gibbs free energy for the phases under study. For the electronic structure the optimized crystal structures were used with a larger set of  $k$ -points. We also used the hybrid HSE06<sup>52-55</sup> exchange-correlation functional to calculate the electronic band structure and the electronic density of states. For these calculations we performed a full reoptimization of the structures obtained with the AM05 exchange correlation functional. In general, we found a difference of less than 1 GPa between the calculations performed with AM05 and HSE06 functionals for a specific volume.

### 3 Results and Discussion

#### 3.1 Structure of experimentally known polymorphs of $\text{InVO}_4$

According to the literature,  $\text{InVO}_4$  has been successfully synthesized and characterized in three different polymorphs, the  $\alpha$ - $\text{MnMoO}_4$ -type ( $\text{InVO}_4$ -I),<sup>27,28</sup> the  $\text{CrVO}_4$ -type structure ( $\text{InVO}_4$ -III),<sup>24,25</sup> and, most recently, the wolframite ( $\text{InVO}_4$ -V).<sup>25</sup> While phases I and III crystallize at ambient pressure, phase V was recently identified just under pressure.<sup>25</sup> Also, lately *ab initio* calculations were used to study phases III and V.<sup>29</sup> In order to determine the crystal structure and the relative stability of these phases at ambient and high pressure, we carry out the calculations of the simulations of these phases at different volumes.

The equilibrium volume and unit-cell parameters were calculated by minimizing the crystal total energy for different volumes allowing to relax the internal atomic positions and lattice parameters. The volume-energy data were fitted with a third-order Birch-Murnaghan

equation of state (EOS).<sup>56</sup> As is shown in Fig. 2 (a) and (b) the lowest energy structure of  $\text{InVO}_4$  belongs to the  $\text{CrVO}_4$ -type structure followed by the  $\alpha$ - $\text{MnMoO}_4$ -type structure and wolframite. Table 1 presents the optimized structural parameters obtained from our calculations, the theoretical results from Mondal *et al.*<sup>29</sup> and the experimental values published in the literature<sup>25,27-29</sup> for comparison. For each phase, the pressure at which the values have been taken is indicated. As expected from a GGA exchange correlation functional, there is a small overestimation of the calculated equilibrium volume with respect to experimental values. In the present case there is a good agreement with a difference of less than 1.5% in the lattice parameters with respect to experimental values. Note that the corresponding difference between the results from Mondal *et al.*<sup>29</sup> and the experimental data from Ref. 25 is of the order of 3%, which represents a difference in the equilibrium volume of  $\approx 7.4\%$ . Also, our results, of bulk modulus ( $B_0$ ) and bulk pressure derivative ( $B_0'$ ), are in better agreement than those from Mondal *et al.*<sup>29</sup> with respect to the experimental results from Ref. 25. For wolframite, the experimental parameters were obtained above 8 GPa, since the ambient pressure values obtained from experiments are unknown due to the mixture of phases III and V observed once pressure is released from 23.9 GPa.<sup>25</sup> In the next section we will deal with the stability of these phases under pressure.

Reports related to the  $\text{InVO}_4$ -I phase are limited to the work performed by Touboul *et al.*<sup>20,26</sup> and Roncaglia *et al.*<sup>27</sup> This phase has not attracted much attention, due to its low stability. However, it is well known that this phase resembles the structure of  $\text{CrVO}_4$ -I<sup>15</sup> and  $\alpha$ - $\text{MnMoO}_4$ .<sup>57</sup> Therefore, a good description of this phase is needed, furthermore it could help to understand the  $\alpha$ - $\text{MnMoO}_4$  compound and other molybdates with the same structure.<sup>58</sup> The  $\text{InVO}_4$ -I phase has eight f.u. in the unit cell. In this structure there are two nonequivalent positions for In and V and five oxygen positions (Table 2), which leads to several different In-O and V-O bond distances, as can be appreciated in Table 3. The values for In-O (V-O) range from 2.092 (1.671) to 2.267 (1.854) Å, in good agreement with experimental results.<sup>28</sup> In this structure, In and V atoms are surrounded by six and

Table 1: Structural parameters and bulk properties of experimentally known polymorphs of  $\text{InVO}_4$  at ambient pressure and high pressures. Where  $a$ ,  $b$ , and  $c$  are the lattice parameters,  $V$  is the volume ( $V/\text{f.u.}$  appear on parenthesis),  $B$  the bulk modulus, and  $B_0'$  the pressure derivative of bulk modulus.

	$\alpha\text{-MnMoO}_4\text{-type}$			$\text{CrVO}_4\text{-type}$			wolframite			$\text{CuWO}_4\text{-type}$	
	DFT <sup>a</sup>	Exp. <sup>28</sup>	Exp. <sup>27</sup>	DFT <sup>a</sup>	DFT <sup>29</sup>	Exp. <sup>25</sup>	DFT <sup>a</sup>	DFT <sup>29</sup>	Exp. <sup>25</sup>	DFT <sup>a</sup>	Exp. <sup>25</sup>
$P$ (GPa)	atm.	atm.	atm.	atm.	atm.	0.8	8.5	6.0	8.2	8.57	8.2
$a$ (Å)	10.3516	10.271	10.49	5.7547	5.816	5.738	4.7009	4.776	4.714	4.6996	4.714
$b$ (Å)	9.4700	9.403	9.39	8.6168	8.739	8.492	5.5197	5.588	5.459	4.8840	5.459
$c$ (Å)	7.0863	7.038	7.12	6.6751	6.775	6.582	4.8849	4.958	4.903	5.5220	4.903
$\alpha$ (deg.)										90.021	90.2
$\beta$ (deg.)	104.81	105.08	105.1				92.62	92.89	93.8	90.030	93.8
$\gamma$ (deg.)										92.588	90.2
$Z$	8	8	8	4	4	4	2	2	2	2	2
$V$ (Å <sup>3</sup> )	671.6	656.3	677.4	331.0	344.37	320.72	126.62	132.17	125.89	126.62	125.89
	(83.95)	(82.04)	(84.67)	(82.75)	(86.09)	(80.18)	(63.31)	(66.08)	(62.94)	(63.31)	(62.94)
$B_0$ (GPa)	120.9			71.0	76.47	69	166.1	183.0	168	166.1	168
$B_0'$	4.52			4.0	3.0	4.0	4.26	6.0	4.0	4.26	4.0

<sup>a</sup> This work.

four oxygen atoms, respectively, to form the irregular  $\text{InO}_6$  octahedra and  $\text{VO}_4$  tetrahedra (Figure 1 a). The four  $\text{InO}_6$  units share edges along  $y$  and  $z$  directions to form  $\text{In}_4\text{O}_{16}$  clusters which share corners with sixteen  $\text{VO}_4$  tetrahedras in such a way that layers of  $\text{In}_4\text{O}_{16}$  clusters are formed separated by  $\text{VO}_4$  units in the  $(20\bar{1})$  plane. The  $\text{VO}_4$  units do not share corners with each other, but are connected to the corners of each  $\text{InO}_6$  octahedra. We have to mention that the formation of these clusters was not observed in the other phases studied in this work.

The  $\text{CrVO}_4\text{-type}$  structure is the most studied phase of  $\text{InVO}_4$ . We just mention that the structure consist of edge-sharing  $\text{InO}_6$  octahedra along the  $c$  direction, the chains are linked together with  $\text{VO}_4$  tetrahedra (Figure 1-a). The tetrahedra and octahedra are more regular than in the  $\alpha\text{-MnMoO}_4$  structure as can be inferred from the In-O and V-O distances displayed in Table 3. The apical distances of the  $\text{InO}_6$  polyhedra are  $2.1392 (\times 2)$  Å and the equatorial are  $2.1877 (\times 4)$  Å. In this structure the  $\text{VO}_4$  tetrahedra are not linked to one another. The In and V atoms occupy  $4a$  and  $4c$  positions, respectively, while there are

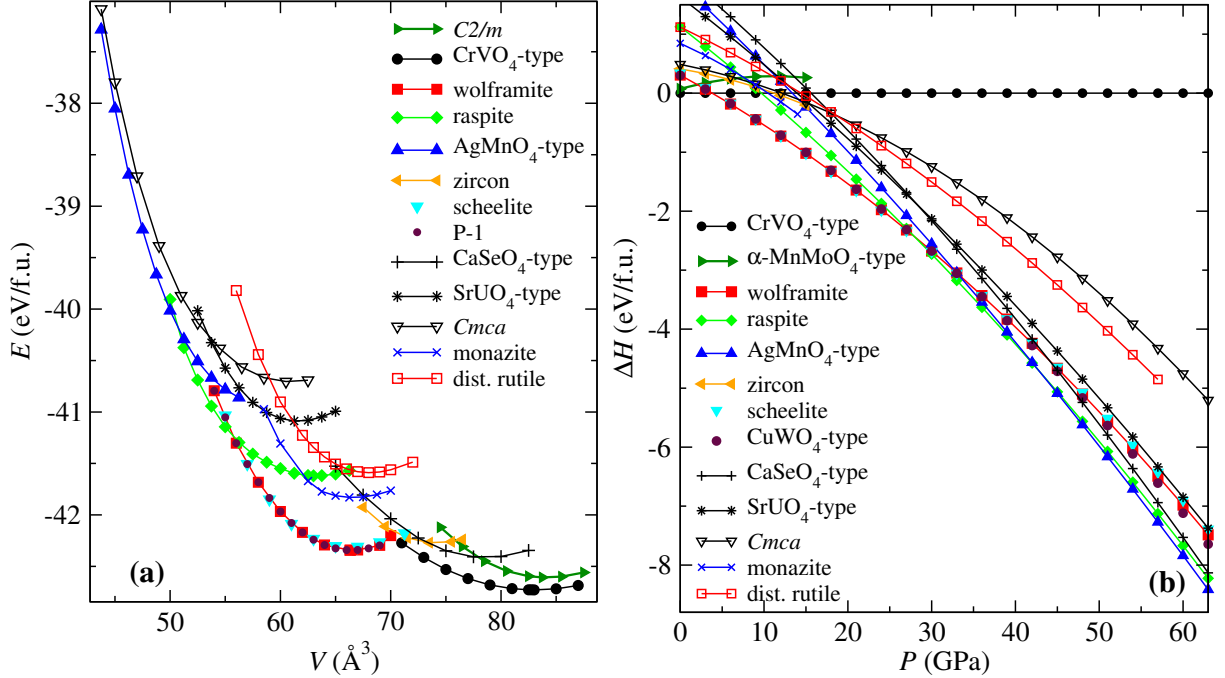


Figure 2: (Color online) (a) Calculated total energy-volume curves for the studied polymorphs of  $\text{InVO}_4$  and (b) pressure dependence of enthalpy for the calculated phases of  $\text{InVO}_4$ .

two nonequivalent oxygen atoms in  $8g$  and  $8f$  positions, see Table 2. As can be seen from Tables 1 to 3 our results are in good agreement with the experimental data reported in Refs. 24 and 25.

The structure of wolframite was widely studied for other compounds that crystallizes in this structure at ambient pressure, such as  $\text{ABO}_4$  [ $A = \text{Mg, Mn, Fe, Co, Ni}$ ,  $B = \text{Mo, W}$ ].<sup>1,30,59–62</sup> Since the experimental data are reported above 8 GPa, our theoretical description of this phase will be done for the structure at 8.5 GPa. At this pressure there are remarkable differences between this phase and the others previously described. From bond distances in Table 3, it can be deduced that polyhedra  $\text{InO}_6$  and  $\text{VO}_6$ , Fig. 1 (c), are more irregular than in phase III. The structure consist of alternating  $\text{InO}_6$  and  $\text{VO}_6$  octahedral units that share edges, forming zigzag chains building a close-packed structure.<sup>30</sup> These alternating chains are the reason of the highest bulk modulus of wolframite in comparison with phases I and III. In this structure, the  $\text{VO}_6$  octahedra are less compressible than the

Table 2: Wyckoff positions of the experimentally known polymorphs of  $\text{InVO}_4$  for values of Table 1.

		$\alpha\text{-MnMoO}_4\text{-type}$					
		DFT			Exp. <sup>28</sup>		
Atom	WP	$x$	$y$	$z$	$x$	$y$	$z$
In <sub>1</sub>	4 <i>h</i>	0	0.1870	0.5	0	0.1875	0.5
In <sub>2</sub>	4 <i>i</i>	0.7892	0	0.1317	0.7907	0	0.1313
V <sub>1</sub>	4 <i>g</i>	0	0.2520	0	0	0.2563	0
V <sub>2</sub>	4 <i>i</i>	0.2737	0	0.4061	0.2737	0	0.402
O <sub>1</sub>	4 <i>i</i>	0.1410	0	0.5394	0.141	0.5	0.541
O <sub>2</sub>	4 <i>i</i>	0.7915	0	0.8374	0.789	0	0.831
O <sub>3</sub>	8 <i>j</i>	0.6324	0.1496	0.1074	0.636	0.153	0.107
O <sub>4</sub>	8 <i>j</i>	0.0481	0.1553	0.8127	0.044	0.161	0.808
O <sub>5</sub>	8 <i>j</i>	0.1393	0.3512	0.5252	0.136	0.350	0.522

		$\text{CrVO}_4\text{-type}$								
		DFT			DFT <sup>29</sup>			Exp. <sup>25</sup>		
Atom	WP	$x$	$y$	$z$	$x$	$y$	$z$	$x$	$y$	$z$
In	4 <i>a</i>	0	0	0	0	0	0	0	0	0
V	4 <i>c</i>	0	0.3581	0.25	0	0.358	0.25	0	0.3617	0.25
O <sub>1</sub>	8 <i>g</i>	0.2575	0.4730	0.25	0.256	0.473	0.25	0.2568	0.4831	0.25
O <sub>2</sub>	8 <i>f</i>	0	0.7543	0.9536	0	0.753	0.953	0	0.7492	0.9573

		wolframite								
		DFT			DFT <sup>29</sup>			Exp. <sup>25</sup>		
Atom	WP	$x$	$y$	$z$	$x$	$y$	$z$	$x$	$y$	$z$
In	2 <i>f</i>	0.5	0.7040	0.25	0.5	0.704	0.25	0.5	0.711	0.25
V	2 <i>e</i>	0	0.1814	0.25	0	0.181	0.25	0	0.159	0.25
O <sub>1</sub>	4 <i>g</i>	0.2128	0.9086	0.4574	0.21	0.91	0.46	0.214	0.861	0.492
O <sub>2</sub>	4 <i>g</i>	0.2499	0.3834	0.3885	0.248	0.382	0.386	0.241	0.407	0.399

		$\text{CuWO}_4\text{-type}$					
		DFT			Exp. <sup>25</sup>		
Atom	WP	$x$	$y$	$z$	$x$	$y$	$z$
In	2 <i>i</i>	0.4999	0.7498	0.2964	0.5	0.711	0.25
V	2 <i>i</i>	0.0004	0.7501	0.8188	0	0.159	0.25
O <sub>1</sub>	2 <i>i</i>	0.7871	0.5429	0.0915	0.214	0.861	0.491
O <sub>2</sub>	2 <i>i</i>	0.2127	0.9569	0.0916	0.786	0.861	0.492
O <sub>3</sub>	2 <i>i</i>	0.7501	0.6117	0.6168	0.242	0.407	0.399
O <sub>4</sub>	2 <i>i</i>	0.2500	0.8884	0.6168	0.758	0.407	0.101

$\text{InO}_6$  polyhedra.<sup>1</sup> This topic will be treated in more detail in the next section.

In order to correlate our results with the experimental ones,<sup>25</sup> we used the coordinates of

Table 3: Interatomic bond distances, In-O and V-O for the experimental known polymorphs of InVO<sub>4</sub>. The experimental data were taken from Refs. 28 and 25.

	In-O (Å)			V-O (Å)	
	DFT	Exp.		DFT	Exp.
$\alpha$ -MnMoO <sub>4</sub> -type					
In <sub>1</sub> -O <sub>1</sub> ( $\times 2$ )	2.2667	2.25	V <sub>1</sub> -O <sub>3</sub> ( $\times 2$ )	1.6714	1.64
In <sub>1</sub> -O <sub>4</sub> ( $\times 2$ )	2.1645	2.11	V <sub>1</sub> -O <sub>4</sub> ( $\times 2$ )	1.7848	1.78
In <sub>1</sub> -O <sub>5</sub> ( $\times 2$ )	2.0969	2.05	V <sub>2</sub> -O <sub>1</sub> ( $\times 1$ )	1.8544	1.87
In <sub>2</sub> -O <sub>1</sub> ( $\times 1$ )	2.2571	2.23	V <sub>2</sub> -O <sub>2</sub> ( $\times 1$ )	1.6856	1.59
In <sub>2</sub> -O <sub>2</sub> ( $\times 1$ )	2.0917	2.11	V <sub>2</sub> -O <sub>5</sub> ( $\times 2$ )	1.6763	1.69
In <sub>2</sub> -O <sub>3</sub> ( $\times 2$ )	2.1276	2.12	$\langle$ In-O $\rangle$	1.7256	1.71
In <sub>2</sub> -O <sub>4</sub> ( $\times 2$ )	2.1947	2.23			
$\langle$ In-O $\rangle$	2.1708	2.155			
CrVO <sub>4</sub> -type					
In-O <sub>2</sub> ( $\times 2$ )	2.1392	2.1483	V-O <sub>2</sub> ( $\times 2$ )	1.6690	1.6579
In-O <sub>1</sub> ( $\times 4$ )	2.1877	2.1623	V-O <sub>1</sub> ( $\times 2$ )	1.7824	1.7983
$\langle$ In-O $\rangle$	2.1755	2.1588	$\langle$ V-O $\rangle$	1.7257	1.7281
CrVO <sub>4</sub> -type <sup>29</sup>					
In-O <sub>2</sub> ( $\times 2$ )	2.22		V-O <sub>2</sub> ( $\times 2$ )	1.68	
In-O <sub>1</sub> ( $\times 4$ )	2.18		V-O <sub>1</sub> ( $\times 2$ )	1.79	
$\langle$ In-O $\rangle$	2.193		$\langle$ V-O $\rangle$	1.735	
wolframite					
In-O <sub>1</sub> ( $\times 2$ )	2.0610	2.0268	V-O <sub>1</sub> ( $\times 2$ )	1.7346	1.6730
In-O <sub>2</sub> ( $\times 2$ )	2.1316	2.1397	V-O <sub>1</sub> ( $\times 2$ )	2.0501	2.2166
In-O <sub>2</sub> ( $\times 2$ )	2.2459	2.2101	V-O <sub>2</sub> ( $\times 2$ )	1.8498	1.8861
$\langle$ In-O $\rangle$	2.1462	2.1255	$\langle$ V-O $\rangle$	1.8782	1.9252
wolframite <sup>29</sup>					
In-O <sub>1</sub> ( $\times 2$ )	2.11		V-O <sub>1</sub> ( $\times 2$ )	1.75	
In-O <sub>2</sub> ( $\times 2$ )	2.18		V-O <sub>1</sub> ( $\times 2$ )	2.08	
In-O <sub>2</sub> ( $\times 2$ )	2.29		V-O <sub>2</sub> ( $\times 2$ )	1.87	
$\langle$ In-O $\rangle$	2.193		$\langle$ V-O $\rangle$	1.90	
CuWO <sub>4</sub> -type					
In-O <sub>1</sub> ( $\times 1$ )	2.0605		V-O <sub>1</sub> ( $\times 1$ )	1.7340	
In-O <sub>2</sub> ( $\times 1$ )	2.0607		V-O <sub>2</sub> ( $\times 1$ )	1.7351	
In-O <sub>3</sub> ( $\times 1$ )	2.1313		V-O <sub>3</sub> ( $\times 1$ )	1.8492	
In-O <sub>4</sub> ( $\times 1$ )	2.1319		V-O <sub>4</sub> ( $\times 1$ )	1.8506	
In-O <sub>5</sub> ( $\times 1$ )	2.2445		V-O <sub>5</sub> ( $\times 1$ )	2.0480	
In-O <sub>6</sub> ( $\times 1$ )	2.2453		V-O <sub>6</sub> ( $\times 1$ )	2.0511	
$\langle$ In-O $\rangle$	2.1457		$\langle$ V-O $\rangle$	1.8780	

the reported triclinic  $P\bar{1}$  structure,<sup>25</sup> which could be described as a  $\text{CuWO}_4$ -type structure (SG:  $P\bar{1}$ , No. 2,  $Z = 2$ , CS: triclinic),<sup>63</sup> to calculate the stability of this phase against the wolframite. As seen in Fig. 2 (a) wolframite and  $\text{CuWO}_4$ -type structure are energetically competitive, as a matter of fact it seems that  $\text{CuWO}_4$ -type structure is a distortion of the wolframite one. According to Table 1 to 3 this distortion is small, so small that the difference in the results for phase transitions and phonons are almost negligible, as we will see in the next sections.

### 3.2 Phase transitions

To the best of our knowledge there are very few studies about the stability of  $\text{InVO}_4$  under extreme conditions of temperature<sup>24</sup> and pressure.<sup>25,29</sup> The X-ray diffraction pattern of  $\text{InVO}_4$  in the  $\text{CrVO}_4$ -type structure was reported from ambient temperature to 1023 K.<sup>24</sup> No phase transition in this range of temperature was reported, only a smooth increase in the unit-cell parameters and a significantly higher conductivity above 723 K were observed. On the other hand, according to the high pressure studies from Ref. 25 the  $\text{InVO}_4$  undergoes a phase transition at 7 GPa from the  $\text{CrVO}_4$ -type structure to the novel polymorph wolframite, which has been designed as phase V of this compound. This phase transition was accompanied by a volume reduction of 14%. Another phase between III and V was also observed in the experiments performed by Errandonea *et al.*<sup>25</sup> This phase IV could not be well described because it appears as a minority phase in the X-ray patterns in a small range of pressure coexisting with phases III and V. As is explained in Ref. 25, phase IV was never observed as a pure phase.

On the other hand, first-principles calculations were used to study the phase transition from  $\text{CrVO}_4$ -type structure to wolframite.<sup>29</sup> Where a phase transition pressure of 5.6 GPa was reported. In their work Mondal *et al.* reported the pressure evolution of lattice parameters, volume and interatomic bond distances for both phases up to a pressure of 14 GPa.<sup>29</sup>

Regarding to the high pressure behavior of other  $\text{ABO}_4$  compounds with  $\text{CrVO}_4$ -type

structure, it has been reported that  $\text{TiPO}_4$  and  $\text{InPO}_4$  follow the phase transition sequence  $\text{CrVO}_4$ -type  $\rightarrow$  zircon  $\rightarrow$  scheelite  $\rightarrow$  wolframite.<sup>33</sup> The first two transitions were also observed in  $\text{TiSiO}_4$ .<sup>64</sup> Besides,  $\text{CaSO}_4$  undergoes the next phase transitions:  $\text{CrVO}_4$ -type  $\rightarrow$  monazite  $\rightarrow$  barite (SG:  $Pbnm$ , No. 62,  $Z = 4$ , CS: orthorhombic)  $\rightarrow$  scheelite.<sup>65</sup> While  $\text{CaSeO}_4$ , which crystallizes in an structure with space group very close to the  $\text{CrVO}_4$ -type structure (SG:  $Cmca$ , No. 64,  $Z = 4$ , CS: orthorhombic), experiments the phase transition sequence  $Cmca \rightarrow$  scheelite  $\rightarrow$   $\text{AgMnO}_4$ -type structure.<sup>66</sup> Otherwise, much less studies have been devoted to study  $\text{FeVO}_4$  and  $\text{CrVO}_4$  under pressure.<sup>67,68</sup>

Going beyond the pressures range achieved in the experiments conducted by Errandonea *et al.*,<sup>25</sup> we analyze the high pressure behavior of  $\text{InVO}_4$  and we consider several possible structures in addition to the known polymorphs reported in the literature. To make the selection of candidates phases we take into consideration the north-east trend followed by other compounds in the Bastide's diagram<sup>1</sup> and previous studies performed in  $\text{ABO}_4$  compounds.<sup>6,33,64-68</sup> Among the selected structures are the zircon, which is the structure of other vanadates such as  $\text{HoVO}_4$ <sup>69</sup> and  $\text{CeVO}_4$ ,<sup>11</sup> and the scheelite,<sup>70</sup> which has been reported as a high pressure phase of several vanadates<sup>71</sup> and some compounds that crystallizes in the  $\text{CrVO}_4$ -structure<sup>33,64,65</sup> and in the  $Cmca$ -type structure.<sup>66</sup>

We have also considered the monazite phase, this structure occurs frequently among  $\text{ABO}_4$  compounds.<sup>14</sup> In particular, this structure is a prototype of high pressure phase of  $\text{CrVO}_4$ -type compounds<sup>6</sup> and has been reported as a high-pressure phase of  $\text{PrVO}_4$ ,<sup>72</sup>  $\text{CaSO}_4$ ,<sup>65</sup> and  $\text{CaSeO}_4$ .<sup>66</sup> Other phases studied such as raspite and  $\text{AgMnO}_4$ -type were found as a post-scheelite phase of  $\text{CaSO}_4$ ,<sup>73</sup>  $\text{CaSeO}_4$ ,<sup>66</sup> and  $\text{SrCrO}_4$ .<sup>74</sup> Some other post-scheelite<sup>33</sup> phase were considered as the  $\text{SrUO}_4$ -type (SG:  $Pbcm$ , No. 57,  $Z = 4$ , CS: orthorhombic) and the distorted (dist.) rutile (SG:  $Cmmm$ , No. 65,  $Z = 2$ , CS: orthorhombic), is a prototype of high pressure phase for  $\text{CrVO}_4$ -type compounds.<sup>6</sup> Two different structures with  $Cmca$  space group (No. 64) were also included in our study, one corresponds to the polymorphous reported of  $\text{CaSeO}_4$  with  $Z = 4$ ,<sup>66</sup> and the other one with 8 f.u. in the unit cell corresponds to

the high-pressure phase reported for some  $AWO_4$  compounds.<sup>1</sup> To compare our results with the experimental data, we take into account the  $CuWO_4$ -type structure.<sup>63</sup> For completeness, we also include the study of the possible decomposition of  $InVO_4$  under pressure to form  $InO + VO_3$ , in order to find if this matches with the experimental data of phase IV.

The calculated energy-volume curves for the mentioned polymorphs of  $InVO_4$  are illustrated in Fig. 2 (a). The relative stability and coexistence pressures of these phases can be extracted by the common-tangent construction.<sup>32</sup> The pressure-enthalpy diagram for the considered structures shows that, besides the known polymorphs of  $InVO_4$ , only the raspite,  $AgMnO_4$ -type, and the  $CuWO_4$ -type are competitive in the high-pressure range, see Fig. 2 (b). Hence, we only calculated the Gibbs energy for these structures. We have to remember that the calculation of Gibbs free energy by the procedure described in Section 2 is computationally expensive, reason for which we only get the Gibbs free energy for the most representative phases of  $InVO_4$ . Figure 3 shows the pressure evolution of the Gibbs energy difference,  $\Delta G$ , for the most representative phases at 300 K.

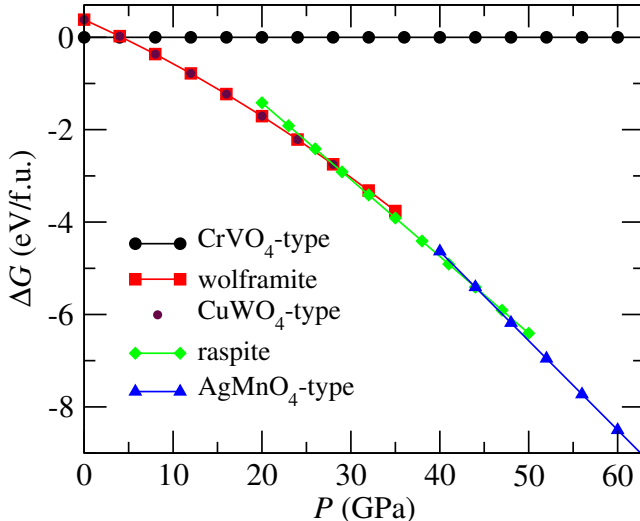


Figure 3: (Color online) Pressure dependence of Gibbs free energy (at 300 K) for the most stable phases of  $InVO_4$ .

According to our calculations, the  $CrVO_4$ -type structure is stable up to 4.4 GPa. For this phase there is a good agreement with the experimental data for the pressure evolution

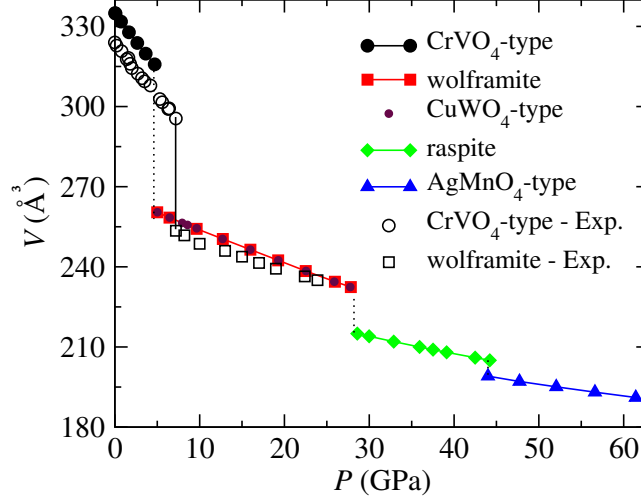


Figure 4: (Color online) Volume curves as function of pressure for the most stable polymorphs of  $\text{InVO}_4$ . The experimental data was taken from Ref. 25. Vertical dotted (continuous) lines show the path followed in the phase transitions obtained from DFT calculations (experiments).

of volume and lattice parameters as is shown in Fig. 4 and 5, respectively. We can see from Fig. 5 that lattice parameter  $b$  is more compressible than  $c$  and  $a$ . This arise from the fact that the  $\text{InO}_6$  unit rotates around the  $y$  axis as pressure increases because the apical interatomic bond distance of  $\text{InO}_6$  polyhedra ( $\text{In-O}_2$  in Fig. 6) is less compressible than equatorial ones ( $\text{In-O}_1$ ); this promotes a shortening in the lattice parameter  $b$ . This behavior, also observed in  $\text{CaSO}_4$ ,<sup>65</sup> differs from that observed in  $\text{TiSiO}_4$ ,<sup>64</sup>  $\text{InPO}_4$ , and  $\text{TiPO}_4$ <sup>33</sup> where the apical  $\text{In-O}_2$  bond distance remains almost constant under pressure. On the other hand, since  $\text{V-O}_2$  distances are oriented in the  $c$  direction, the compression of this axis is due to the reduction of the equatorial bond distances of  $\text{InO}_6$ , as  $\text{V-O}_2$  remain almost constant under pressure.

At 4.4 GPa the  $\text{CrVO}_4$ -type structure undergoes a first order phase transition as can be seen in Fig. 3. Experimentally, prior to the transition to wolframite phase, a transition to a phase IV was observed. However it was not possible to give a description of this structure.<sup>25</sup> According to Fig. 2 (a) scheelite-type and  $\text{CuWO}_4$ -type structure are competitive with wolframite. In order to find the phase IV we compare the simulated X-ray diffraction patterns of these structures with the experimental ones reported in Ref. 25, however the

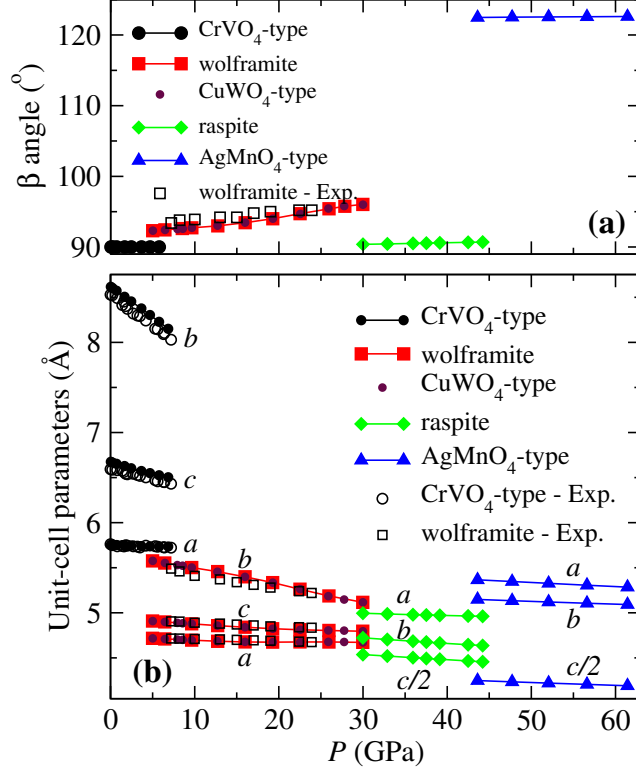


Figure 5: (Color online) Pressure dependence of (a)  $\beta$  angle and (b) lattice parameters for the studied polymorphs of  $\text{InVO}_4$ . The experimental data was taken from Ref. 25.

patterns of scheelite-type structure do not fit with the experimental one. We also compare the simulated X-ray patterns of the products of decomposition of  $\text{InVO}_4$  and we did not find an agreement with the diffraction patterns of  $\text{InO}+\text{VO}_3$ . Hence, the description of phase IV will be left for a future work. According to our results, the wolframite and  $\text{CuWO}_4$ -type structure has almost the same energy, where the  $\text{CuWO}_4$ -type could be considered as a distortion of the wolframite; hence, the crystallographic parameters from the  $\text{CuWO}_4$ -type structure are almost the same as the wolframite, see Table 1 to 3 and Figures 2 to 6. We will see in the next section that phonons from wolframite and the  $\text{CuWO}_4$ -type structure are very similar.

In the transition from  $\text{CrVO}_4$ -type to wolframite,  $\text{InVO}_4$  has a large volume reduction of 17.5%, in good agreement with the experimental value (see Figure 4). This volume reduction is associated with a change in the coordination of the polyhedron around V, from  $\text{VO}_4$  to

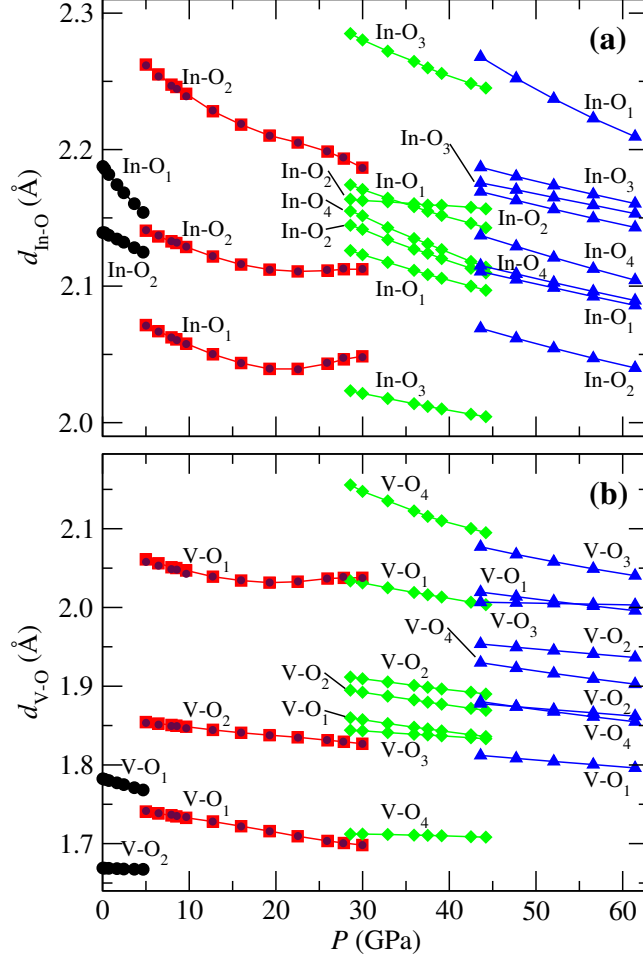


Figure 6: (Color online) Pressure dependence of interatomic bond distances (a) In-O and (b) V-O. Black circles, red squares, purple circles, green diamonds, and blue triangles correspond to  $\text{CrVO}_4$ -type, wolframite,  $\text{CuWO}_4$ -type, raspite, and  $\text{AgMnO}_4$ -type structures, respectively.

$\text{VO}_6$ . Figure 5 shows that the lattice parameters and  $\beta$  angle obtained from calculations are in very good agreement with the experimental results. According to Figure 5b, the lattice parameter  $b$  is much more compressible than  $a$  and  $c$ , here  $a$  almost remains constant. In-O bond lengths in this phase behave in a way similar to that for  $\text{CrVO}_4$ -type. The apical bond distance (In-O<sub>2</sub> in the middle zone of Figure 6a) is less compressible than the other In-O bond distances. As seen in Figure 6, a change in the slope of the pressure dependence of interatomic bond distances V-O<sub>1</sub> and In-O starts at 14 GPa. These changes are not reflected in the lattice parameters but they play an important role in the vibrational properties that

will be discussed in section 3.3.

According to Fig. 3 the wolframite phase is stable up to 28.1 GPa, then  $\text{InVO}_4$  presents a transition to the raspite structure (phase VI). This transition is accompanied of a volume reduction of 7.5 %. Experiments on  $\text{InVO}_4$  were conducted only up to 24 GPa,<sup>25</sup> reason for which this phase transition was not observed. The lattice parameters of raspite for a volume of  $212 \text{ \AA}^3$  and a pressure of 32.9 GPa are  $a = 4.9869 \text{ \AA}$ ,  $b = 4.7032 \text{ \AA}$ ,  $c = 9.0390 \text{ \AA}$ , and  $\beta = 90.51^\circ$ . In this structure all the non equivalent atoms are located in the  $4e$  WP: In (0.5334, 0.2408, 0.6182), V (0.03432, 0.2457, 0.8893), O1 (0.2290, 0.9886, 0.03418), O2 (0.2089, 0.003844, 0.5248), O3 (0.3813, 0.2795, 0.8235), and O4 (0.09154, 0.8490, 0.7789). We found from the EOS a bulk modulus of  $B_0 = 112.72 \text{ GPa}$  with  $V_0 = 252.77 \text{ \AA}^3$  and  $B_0' = 4.25$ . From lattice parameters and  $\beta$  angle presented in Fig.5 we observe that this phase resembles a distorted tetragonal structure, it consists of alternating zig-zag chains of  $\text{InO}_7$  polyhedra in the  $z$  direction linked by  $\text{VO}_7$  units.  $\text{InO}_7$  polyhedra share edges in the zig-zag chains running perpendicular to plane  $[010]$ , whereas they just share the corners in the  $z$  direction. The same behavior was observed for  $\text{VO}_7$  polyhedra. Figure 6 shows that both In-O and V-O interatomic bond distances have similar compressibility, except for one V- $\text{O}_4$  and one In- $\text{O}_2$  bond distances that are almost constants in all the range of pressure stability.

As pressure increases, raspite becomes unstable and  $\text{InVO}_4$  undergoes a phase transition to the  $\text{AgMnO}_4$ -type structure at 44 GPa (phase VII). As can be seen in Fig. 4 there is just a small volume reduction in the transition from raspite to the  $\text{AgMnO}_4$ -type structure,  $\Delta V = -2.9 \%$ . At 52 GPa the lattice parameters of this phase are  $a = 5.3266 \text{ \AA}$ ,  $b = 5.1199 \text{ \AA}$ ,  $c = 8.4399 \text{ \AA}$ , and  $\beta = 122.56^\circ$ , the volume  $194 \text{ \AA}^3$ . The Figure 5 shows that although raspite and  $\text{AgMnO}_4$ -type phases belongs to the same SG, they have marked differences in the lattice parameters, however they have almost the same compressibility. This is also reflected in the change of interatomic bond distances as function of pressure. Like in raspite, in this phase the In, V, and O atoms are located in the  $4e$  WP as follow: In (0.3725, 0.06524, 0.12899), V (0.9727, 0.005625, 0.6706), O1 (0.7477, 0.9612, 0.4191), O2 (0.9497, 0.3533, 0.5960), O3

(0.3198, 0.2113, 0.8709), and O4 (0.7676, 0.2088, 0.7487). This phase is formed by  $\text{InO}_8$  and  $\text{VO}_8$  units that shares edges and corners. The  $\text{InO}_8$  polyhedra forms layers that lay in the  $bc$  plane, separated by layers formed by  $\text{VO}_8$  polyhedra. We found that  $\text{InVO}_4$  is stable in this phase up to 62 GPa, which is the highest pressure reached in this study.

### 3.3 Vibrational properties

Nowadays the lattice vibration studies, through the analysis of Raman (R) and Infrared (IR) spectra from experimental as well as theoretical methods, have become fundamental tools to understand the behavior of materials at ambient conditions and under extreme conditions of temperature and pressure.<sup>32,49</sup> In particular, these studies help to determine and realize whether a phase transition takes place. In many cases the experimental and theoretical approximations are conjugated with great success to study  $\text{AVO}_4$  compounds, see for example references 11, 75, 72, 76 and references there in; whereas in other circumstances the theoretical results serve as a guide for future experimental and theoretical studies.<sup>33,66</sup> In this section we analyze the lattice dynamics of  $\text{InVO}_4$  in the phases III, V, raspite (VI) and  $\text{AgMnO}_4$ -type (VII) by means of the calculated phonon frequencies at  $\Gamma$  point for each phase, their pressure dependence, and Grüneisen parameters as well as their dispersion relation along the Brillouin zone and phonon DOS.

The calculated and experimental R and IR frequencies at  $\Gamma$  point for the studied phases appear in Table 4 to 6, the pressure coefficients ( $d\omega/dP$ ,) and Grüneisen parameters [ $\gamma = -\partial (\ln \omega)/\partial(\ln V)$ ] were also included. The phonon relation of dispersion and the phonon DOS are displayed in Fig. 7. The vibrational modes of  $\text{InVO}_4$  can be classified as internal or external modes of the  $\text{VO}_4$  unit. The external modes correspond either to a pure translation ( $T$ ) or to a pure rotation ( $R$ ) of the  $\text{VO}_4$  unit. Whereas the internal modes of the  $\text{VO}_4$  tetrahedra are  $\nu_1$  (symmetric stretching),  $\nu_2$  (symmetric bending),  $\nu_3$  (asymmetric stretching), and  $\nu_4$  (asymmetric bending).<sup>33</sup> The  $T$  modes are usually the lowest in frequency, the  $\nu_x$  modes are the highest in frequency, and the frequencies of the  $R$  modes are between those

Table 4: Calculated Raman and infrared phonon frequencies for CrVO<sub>4</sub>-type phase (at ambient pressure) and wolframite phase (at 6.44 GPa) of InVO<sub>4</sub> at the  $\Gamma$  point. Frequencies  $\omega$  are in cm<sup>-1</sup> and  $d\omega/dP$  in cm<sup>-1</sup>/GPa.

	CrVO <sub>4</sub> -type						wolframite						CuWO <sub>4</sub> -type		
	DFT			Exp. <sup>25</sup>			DFT			Exp. <sup>25</sup>			DFT		
	$\omega$	$d\omega/dp$	$\gamma$	$\omega$	$d\omega/dp$		$\omega$	$d\omega/dp$	$\gamma$	$\omega$	$d\omega/dp$		$\omega$	$d\omega/dp$	$\gamma$
$T(B_{3g})$	128.36	1.47	0.37	135	2.1	$B_g$	108.15	0.13	0.24	109	1.8	$A_g$	108.15	0.12	0.22
$T(B_{1g})$	153.78	-2.38	-0.60	191	0.7	$A_g$	124.43	0.05	0.08	118	1.9	$A_g$	124.39	0.05	0.08
$T(A_g)$	193.24	0.27	0.07	218	4.5	$B_g$	139.17	0.75	1.04	145	2.0	$A_g$	139.24	0.76	1.05
$R(B_{1g})$	208.32	4.93	1.24	252	3.6	$B_g$	189.11	1.42	1.44	149	-0.1	$A_g$	189.01	1.43	1.45
$R(B_{2g})$	237.68	3.88	0.98	342	0.4	$B_g$	214.33	1.74	1.55	204	1.5	$A_g$	214.26	1.77	1.57
$\nu_2(A_g)$	334.48	0.37	0.09	348	5.6	$A_g$	241.95	-0.52	-0.43	223	2.2	$A_g$	242.18	-0.58	-0.48
$R(B_{3g})$	352.16	5.01	1.27	377	1.9	$B_g$	289.68	1.06	0.71	241	0.0	$A_g$	289.61	1.07	0.72
$\nu_4(B_{1g})$	361.53	1.38	0.35	389	4.4	$A_g$	304.06	0.74	0.47	251	1.1	$A_g$	304.26	0.72	0.46
$\nu_2(B_{2g})$	370.74	4.64	1.17	390	1.4	$A_g$	340.75	1.23	0.70	319	1.2	$A_g$	340.99	1.13	0.65
$\nu_4(A_g)$	380.68	1.33	0.34	456	5.2	$B_g$	379.81	1.95	1.00	336	2.4	$A_g$	379.61	1.95	0.99
$\nu_4(B_{3g})$	422.85	6.14	1.55	637	7.2	$A_g$	420.14	1.90	0.88	347	1.6	$A_g$	420.11	1.88	0.87
$\nu_3(B_{1g})$	657.99	7.59	1.92	755	5.7	$B_g$	440.53	3.87	1.67	378	1.9	$A_g$	440.39	3.87	1.67
$\nu_3(A_g)$	752.49	6.36	1.61	847	4.2	$B_g$	499.37	3.37	1.30	433	2.0	$A_g$	499.34	3.39	1.30
$\nu_1(A_g)$	920.05	1.33	0.34	914	1.3	$A_g$	520.75	2.32	0.86	531	1.8	$A_g$	520.79	2.29	0.85
$\nu_3(B_{3g})$	925.12	2.34	0.59	918	2.1	$B_g$	679.84	5.04	1.41	684	5.1	$A_g$	679.70	5.13	1.44
						$A_g$	712.73	4.22	1.14	723	3.8	$A_g$	712.93	4.20	1.13
						$B_g$	740.12	5.15	1.33	758	5.2	$A_g$	740.05	5.20	1.34
						$A_g$	835.15	4.62	1.07	850	4.4	$A_g$	836.02	4.62	1.06
$T(B_{1u})$	102.64	0.14	0.04			$B_u$	72.15	-7.61	-11.97			$A_u$	72.49	-7.98	-14.00
$T(B_{3u})$	150.91	-2.09	-0.53			$A_u$	175.83	-0.08	-0.09			$A_u$	176.03	-0.17	-0.20
$T(B_{1u})$	152.31	0.85	0.22			$B_u$	200.95	-0.05	-0.05			$A_u$	201.02	-0.08	-0.07
$T(B_{2u})$	214.39	0.20	0.05			$B_u$	267.83	-0.43	-0.32			$A_u$	267.80	-0.45	-0.33
$R(B_{3u})$	253.72	4.42	1.13			$A_u$	293.65	-0.34	-0.23			$A_u$	293.68	-0.38	-0.25
$T(B_{2u})$	253.85	1.21	0.31			$B_u$	316.80	2.58	1.55			$A_u$	316.73	2.58	1.55
$\nu_4(B_{3u})$	328.31	2.06	0.52			$A_u$	361.33	-0.60	-0.33			$A_u$	361.33	-0.61	-0.33
$R(B_{1u})$	346.36	6.73	1.71			$B_u$	366.10	1.75	0.93			$A_u$	365.90	1.74	0.92
$\nu_2(B_{2u})$	358.37	-0.03	-0.01			$A_u$	456.57	3.04	1.28			$A_u$	456.67	3.01	1.26
$\nu_4(B_{2u})$	396.86	3.69	0.94			$B_u$	497.00	3.84	1.48			$A_u$	496.97	3.85	1.48
$\nu_4(B_{1u})$	423.21	4.95	1.26			$B_u$	531.83	4.27	1.53			$A_u$	531.79	4.31	1.54
$\nu_3(B_{3u})$	681.81	7.29	1.86			$A_u$	544.80	3.75	1.32			$A_u$	544.90	3.74	1.31
$\nu_1(B_{2u})$	758.20	6.59	1.68			$A_u$	610.39	4.98	1.56			$A_u$	610.49	5.04	1.57
$\nu_3(B_{1u})$	893.20	1.72	0.44			$B_u$	697.88	5.14	1.41			$A_u$	698.08	5.27	1.44
$\nu_3(B_{2u})$	936.59	0.94	0.24			$A_u$	761.40	3.91	1.00			$A_u$	760.86	3.95	1.00

of the  $T$  and  $\nu_x$  modes.

According to the group theory analysis, the  $Cmcm$  space group of CrVO<sub>4</sub>-type structure

Table 5: Calculated Raman frequencies for raspite (at 30 GPa) and AgMnO<sub>4</sub>-type structure (at 47.7 GPa) of InVO<sub>4</sub> at the  $\Gamma$  point. Frequencies  $\omega$  are in cm<sup>-1</sup> and  $d\omega/dP$  in cm<sup>-1</sup>/GPa.

raspite				AgMnO <sub>4</sub> -type			
	$\omega$	$d\omega/dp$	$\gamma$		$\omega$	$d\omega/dp$	$\gamma$
$B_g$	149.38	0.02	0.03	$B_g$	141.70	0.26	0.60
$A_g$	154.28	0.55	0.88	$A_g$	153.75	0.51	1.15
$B_g$	160.19	0.89	1.41	$B_g$	172.96	0.43	0.98
$A_g$	160.95	0.68	1.08	$A_g$	189.07	0.60	1.36
$B_g$	175.50	0.51	0.81	$A_g$	199.15	0.36	0.82
$A_g$	188.77	0.64	1.01	$B_g$	224.80	0.69	1.56
$A_g$	196.31	1.51	2.39	$A_g$	241.85	0.98	2.23
$A_g$	230.57	1.69	2.67	$B_g$	308.66	0.83	1.88
$B_g$	268.70	1.31	2.08	$A_g$	312.23	0.61	1.40
$B_g$	272.34	1.50	2.37	$A_g$	332.98	1.34	3.06
$A_g$	287.58	1.36	2.15	$B_g$	349.16	1.05	2.40
$A_g$	306.89	1.82	2.87	$A_g$	362.50	1.29	2.95
$B_g$	313.30	0.81	1.28	$A_g$	383.38	1.31	2.98
$B_g$	317.27	1.79	2.83	$B_g$	388.12	1.35	3.08
$A_g$	366.91	1.39	2.20	$A_g$	430.25	1.32	3.00
$A_g$	376.11	1.58	2.51	$B_g$	434.29	1.33	3.04
$B_g$	382.82	1.48	2.34	$A_g$	465.14	1.11	2.53
$B_g$	395.89	0.97	1.54	$B_g$	471.55	1.36	3.09
$A_g$	399.66	0.63	1.00	$B_g$	474.75	1.50	3.42
$B_g$	404.40	1.80	2.84	$A_g$	485.99	1.78	4.05
$A_g$	448.47	1.51	2.39	$B_g$	502.54	1.45	3.31
$B_g$	472.82	1.74	2.75	$B_g$	530.49	1.65	3.76
$A_g$	481.82	1.56	2.46	$A_g$	555.38	1.93	4.40
$B_g$	503.14	1.76	2.78	$A_g$	563.88	2.49	5.68
$A_g$	519.02	1.80	2.85	$B_g$	568.75	1.94	4.43
$B_g$	549.77	2.26	3.58	$B_g$	593.57	1.60	3.64
$B_g$	630.57	2.60	4.12	$B_g$	636.40	1.94	4.41
$A_g$	638.81	2.73	4.33	$A_g$	640.11	1.84	4.19
$B_g$	683.74	2.26	3.58	$A_g$	695.62	2.25	5.12
$A_g$	729.24	2.45	3.87	$B_g$	719.83	2.02	4.61
$B_g$	729.71	2.45	3.87	$B_g$	724.57	2.46	5.62
$A_g$	750.96	2.51	3.98	$A_g$	738.48	2.32	5.28
$A_g$	784.38	1.91	3.02	$B_g$	773.84	2.43	5.53
$A_g$	817.94	2.78	4.41	$A_g$	778.88	2.33	5.30
$B_g$	821.21	3.05	4.83	$B_g$	825.34	2.41	5.50
$B_g$	902.50	2.00	3.17	$A_g$	863.67	2.39	5.46

has the following representation at  $\Gamma$  point:  $\Gamma = 5A_g + 4B_{1g} + 6B_{1u} + 3A_u + 2B_{2g} + 7B_{2u} + 4B_{3g} + 5B_{3u}$ . Where there are three acoustic modes:  $B_{1u}$ ,  $B_{2u}$ , and  $B_{3u}$ , three silent modes

Table 6: Calculated infrared frequencies for raspite (at 30 GPa) and AgMnO<sub>4</sub>-type structure (at 47.7 GPa) of InVO<sub>4</sub> at the  $\Gamma$  point. Frequencies  $\omega$  are in cm<sup>-1</sup> and  $d\omega/dP$  in cm<sup>-1</sup>/GPa.

	raspite			AgMnO <sub>4</sub> -type			
	$\omega$	$d\omega/dp$	$\gamma$	$\omega$	$d\omega/dp$	$\gamma$	
$B_u$	80.13	0.57	0.91	$A_u$	159.25	0.67	1.53
$A_u$	106.41	0.84	1.34	$A_u$	193.84	0.58	1.33
$A_u$	119.36	0.82	1.29	$B_u$	195.88	0.61	1.40
$B_u$	176.56	1.14	1.81	$B_u$	249.45	1.16	2.66
$A_u$	183.84	0.69	1.09	$A_u$	253.19	0.94	2.16
$B_u$	225.00	0.56	0.89	$A_u$	278.71	1.05	2.40
$A_u$	243.98	1.27	2.01	$B_u$	289.05	1.21	2.77
$A_u$	260.53	2.42	3.83	$A_u$	333.88	0.98	2.24
$B_u$	289.55	1.65	2.62	$A_u$	361.07	1.13	2.59
$A_u$	289.91	1.05	1.67	$B_u$	366.60	1.62	3.70
$B_u$	312.00	1.59	2.51	$A_u$	387.75	0.89	2.05
$A_u$	330.01	1.38	2.19	$B_u$	393.32	1.40	3.21
$B_u$	339.55	2.37	3.75	$A_u$	424.11	1.71	3.90
$A_u$	357.23	1.94	3.08	$B_u$	435.82	1.01	2.32
$B_u$	379.75	0.88	1.40	$A_u$	451.90	2.28	5.22
$A_u$	401.66	1.68	2.66	$B_u$	453.84	1.59	3.63
$B_u$	420.91	2.45	3.89	$B_u$	464.04	1.91	4.37
$A_u$	443.83	1.88	2.98	$A_u$	476.15	1.29	2.94
$B_u$	455.67	2.06	3.26	$B_u$	505.51	1.40	3.20
$A_u$	491.46	2.09	3.31	$A_u$	508.74	2.16	4.93
$B_u$	493.27	2.02	3.20	$B_u$	560.65	1.58	3.60
$B_u$	522.22	2.75	4.35	$B_u$	601.75	1.81	4.15
$A_u$	526.72	2.15	3.41	$A_u$	623.33	1.71	3.91
$B_u$	548.07	1.93	3.05	$B_u$	629.23	1.96	4.48
$A_u$	555.61	2.01	3.19	$A_u$	650.58	2.29	5.23
$A_u$	605.22	2.39	3.78	$B_u$	659.22	2.11	4.82
$B_u$	606.18	2.22	3.51	$A_u$	680.57	1.91	4.36
$B_u$	676.83	2.50	3.96	$B_u$	724.84	2.36	5.38
$A_u$	701.39	2.73	4.33	$A_u$	732.64	2.38	5.43
$B_u$	765.13	2.73	4.33	$B_u$	776.58	2.19	4.99
$A_u$	790.99	2.16	3.43	$A_u$	795.32	2.39	5.47
$A_u$	840.92	2.64	4.18	$A_u$	813.90	2.23	5.10
$B_u$	850.70	2.45	3.87	$B_u$	815.64	2.60	5.93

$A_u$ , 15 infrared active modes:  $5B_{1u}$ ,  $6B_{2u}$ , and  $4B_{3u}$ , and 15 Raman active modes:  $5A_g$ ,  $4B_{1g}$ ,  $2B_{2g}$ , and  $4B_{3g}$ .<sup>33</sup> As can be seen in Table 4 this phase presents two  $T$  and one  $\nu_2$  phonons that are characterized by a decrease of the vibrational frequency with pressure, i.e. negative

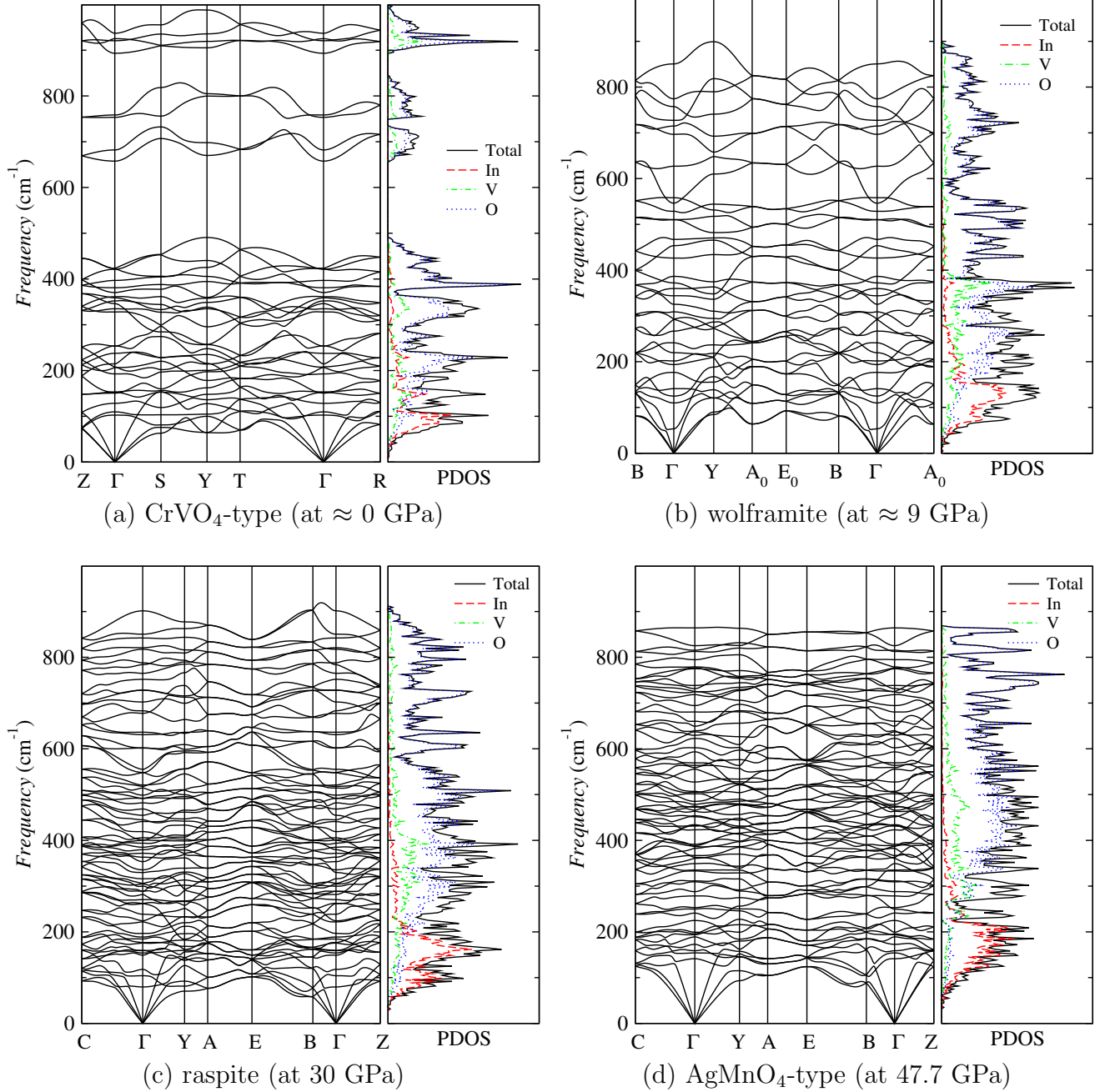


Figure 7: (Color online) Phonon spectrum and phonon DOS of InVO<sub>4</sub> polymorphs: (a) CrVO<sub>4</sub>-type (at  $\approx 0$  GPa), (b) wolframite (at  $\approx 9$  GPa), (c) raspite (at 30 GPa), and (d) AgMnO<sub>4</sub>-type (at 47.7 GPa).

pressure coefficients and Grüneisen parameters, the Raman mode  $B_{1g}$  ( $153.78 \text{ cm}^{-1}$ ) and two IR modes:  $B_{3u}$  ( $150.91 \text{ cm}^{-1}$ ) and  $B_{2u}$  ( $358.37 \text{ cm}^{-1}$ ). The softening of this  $B_{1g}$  Raman ( $B_{3u}$  IR) mode was also observed in CaSO<sub>4</sub><sup>65</sup> (InPO<sub>4</sub>)<sup>33</sup> and could be related with the instability

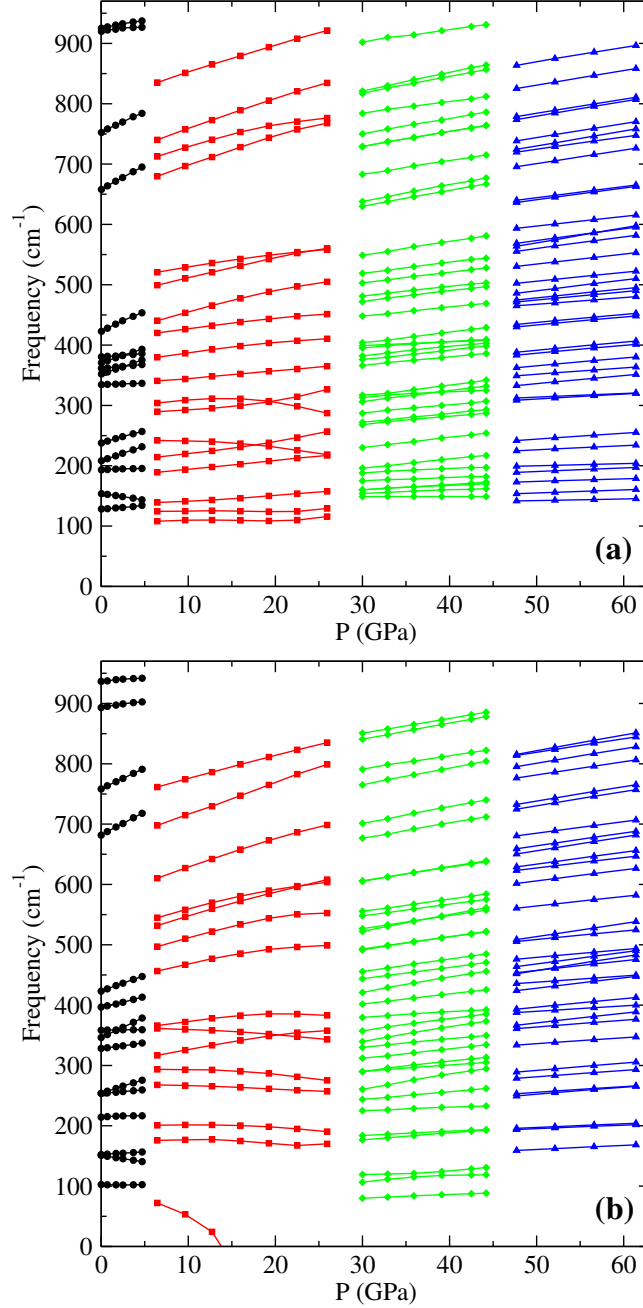


Figure 8: (Color online) Pressure dependence of (a) Raman and (b) IR frequencies of InVO<sub>4</sub>. Black circles, red squares, green diamonds, and blue triangles corresponds to CrVO<sub>4</sub>-type, wolframite, raspite and AgMnO<sub>4</sub>-type structures, respectively.

of the CrVO<sub>4</sub>-type structure under pressure. The pressure evolution of Raman and IR modes of the studied phases is displayed in Fig. 8 (a) and (b), respectively. The phonon dispersion for CrVO<sub>4</sub>, Fig. 7 (a), shows no imaginary frequency. We also realized simulation of phonon

dispersions up to  $\approx 7$  GPa and no significant changes were observed. As seen on the phonon DOS, phonons above  $600 \text{ cm}^{-1}$  belong to internal  $\nu_x$  modes, i.e. there are only contributions from V and O. The frequencies of the external modes are located below  $255 \text{ cm}^{-1}$ , and the intermediate is occupied by external ( $R$ ) and internal ( $\nu$ ) modes.

For wolframite the group theory predicts the following  $\Gamma$  phonon modes:  $\Gamma = 8A_g + 10B_g + 8A_u + 10B_u$ . Here  $2B_u$  and one  $A_u$  infrared modes are acoustic, 18 are Raman ( $8A_g + 10B_g$ ) and 15 are infrared ( $7A_u + 9B_u$ ). The group theory predicts the same modes for  $\text{CuWO}_4$ -type structure at  $\Gamma$  point. According to Table 4 both phases wolframite and  $\text{CuWO}_4$ -type structure presents almost the same phonon frequencies at 6.44 GPa. Besides, we observed that phonon spectrum for both phases are very similar, reason for which we only include the spectrum from wolframite.

Figure 8 (a) shows that the slope of some Raman modes of wolframite starts to change around 16 GPa, so that we calculated the pressure coefficients and Grüneisen parameters from Table 4 by considering just the frequencies from 6 to 14 GPa which correspond to the linear trend for wolframite phase. This change in the frequencies of wolframite is due to a shift in the slope of the  $\text{In-O}_x$  and  $\text{V-O}_1$  interatomic bond distances as pressure increases, see Fig. 6. Having in mind this, we see that wolframite presents several R and IR phonon modes with negative pressure coefficients. It is noteworthy that  $B_u$  IR mode softens completely around 14 GPa, to our knowledge this behavior was not observed previously in other  $\text{CrVO}_4$ -type compounds. However, it has been also reported that this mode softens in the wolframite high-pressure phase of  $\text{InPO}_4$  and  $\text{TiPO}_4$ ,<sup>33</sup> and in other compounds that crystallizes at ambient pressure in the wolframite structure such as  $\text{MgWO}_4$ <sup>59</sup> and  $\text{InTaO}_4$ .<sup>77</sup> The Figure 7 (b) shows the phonon spectra and phonon DOS of wolframite at  $\approx 9$  GPa. We have to mention that we had to perform more calculations of the phonon spectrum with bigger supercells in specific directions of the BZ in order to eliminate possible errors from the supercell method with the PHONON program. On the other hand, above 14 GPa the  $B_u$  IR mode has imaginary frequency at  $\Gamma$  point but also in other special and intermediate points

of the BZ. In another way, the phonon spectrum does not present imaginary frequencies once In is eight-fold coordinated above 34 GPa. We see from Fig. 7 (b) that in this phase of InVO<sub>4</sub> it is not depicted the phonon gap observed in the wolframite of InPO<sub>4</sub> and TiPO<sub>4</sub>.<sup>33</sup>

Group theory predicts that raspite and AgMnO<sub>4</sub>-type structures have the following vibrational representation for R and IR phonon modes at the  $\Gamma$  point:  $\Gamma = 18B_g + 18A_g + 16B_u + 17A_u$ , i.e. 36 R and 33 IR active modes. As we can see from Tables 5 and 6 and from Fig. 8 that all Raman and IR phonon modes shift to higher frequencies upon compression, i.e. the pressure coefficients and Grüneisen parameters are positive. The phonon spectrum for these phases no present imaginary frequencies in all the range of pressure studied. For these phases there is not a gap in the phonon DOS like happens in other compounds with these structures such as CaSeO<sub>4</sub>.<sup>66</sup> In these phases there is not a clear separation of the internal and external modes due to the high coordination of In and V, also because their interatomic bond distances are different between each other, see the contributions of In and V to the phonon DOS of Fig. 7.

### 3.4 Electronic properties

Density functional theory has been used with success to describe the electronic structure of ABO<sub>4</sub> compounds.<sup>11,60,78</sup> In particular, optical-absorption measurements in conjunction with *ab initio* calculations were used to study the electronic structure of zircon-type vanadates as function of pressure.<sup>11,79</sup> However, it is well known that first principles calculations at the level of GGA underestimates the electronic band gap.<sup>80</sup> Hence, some other approximations can be used in order to get a better estimation of the electronic band gap value, like GGA+*U*,<sup>81</sup> *GW*<sup>82</sup> or using hybrid functionals like HSE03 or HSE06.<sup>55,83</sup> Nevertheless, calculations with *GW* or with hybrid functionals require much more computer time than the calculations with GGA or GGA+*U*. So, their use in the community is still limited.

According to the literature, an experimental electronic band gap value of 3.2 eV was reported for a thin-film of InVO<sub>4</sub>-III.<sup>22</sup> While, theoretical calculations of bulk InVO<sub>4</sub>-III

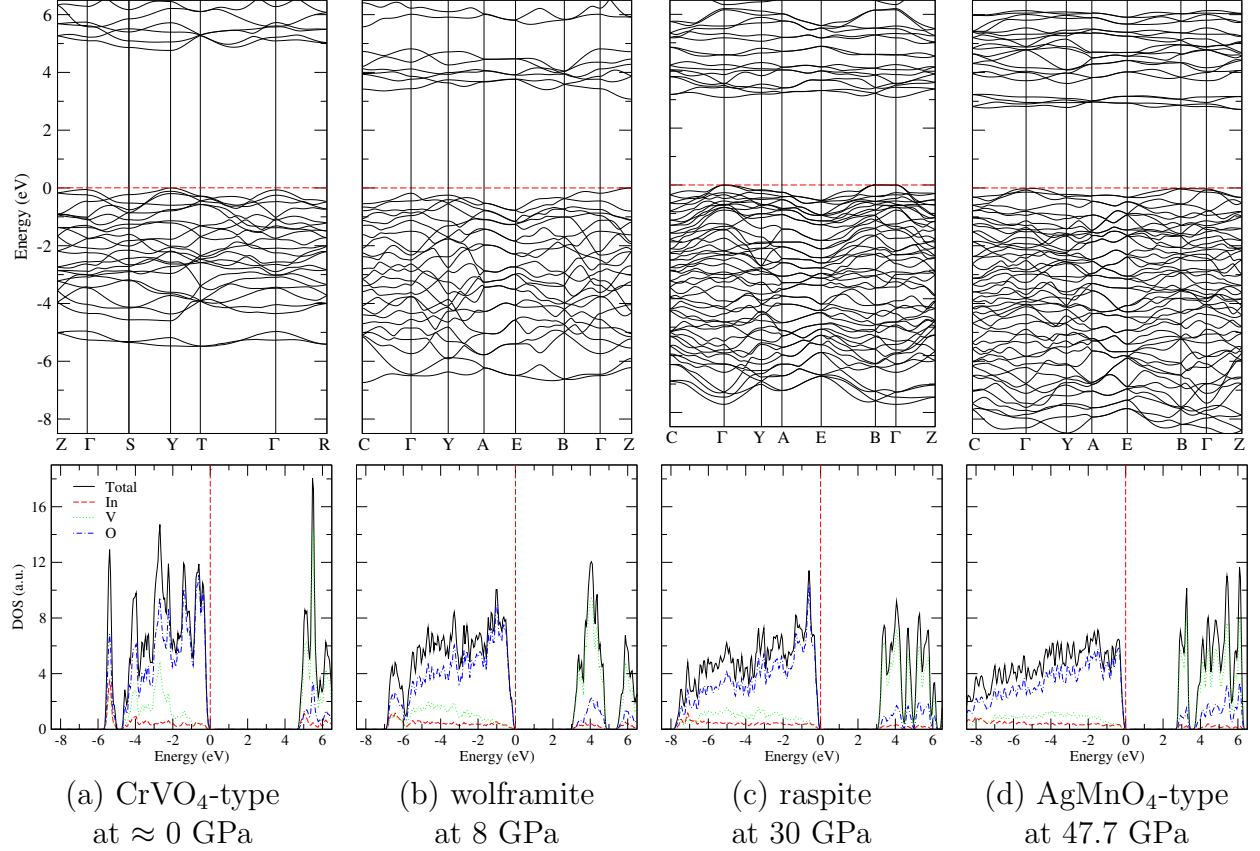


Figure 9: (Color online) Band structure and partial density of states (DOS) of the most stable polymorphs of InVO<sub>4</sub>: (a) CrVO<sub>4</sub>-type (at  $\approx 0$  GPa), (b) wolframite (at 8 GPa), (c) raspite (at 30 GPa), and (d) AgMnO<sub>4</sub>-type (at 47.7 GPa).

performed with WIEN2k code using PBE<sup>84</sup> and Tran-Blaha Modified Becke-Johnson (TB-mBJ)<sup>29</sup> exchange correlation functionals, reported a direct Y-Y electronic band gap of 3.24 and 4.02 eV, respectively. On the other hand, Li *et al.*<sup>84</sup> took the experimental data from Ref. 22 and use the Lambert-Beer's law<sup>85</sup> to determine that the experimental electronic band gap of InVO<sub>4</sub> should be 3.8 eV. These results would comply with the fact that the electronic band gap that is obtained at the GGA level is always lower than that observed experimentally. Given the observed differences in the value of the electronic band-gap, we consider that this compound should be studied again both experimentally as well as theoretically.

In this section we describe the results about the electronic structure of the most stable polymorphs of InVO<sub>4</sub> and the pressure evolution of the energy gap. In order to obtain a better description of electronic structure, we performed the calculations by using the HSE06

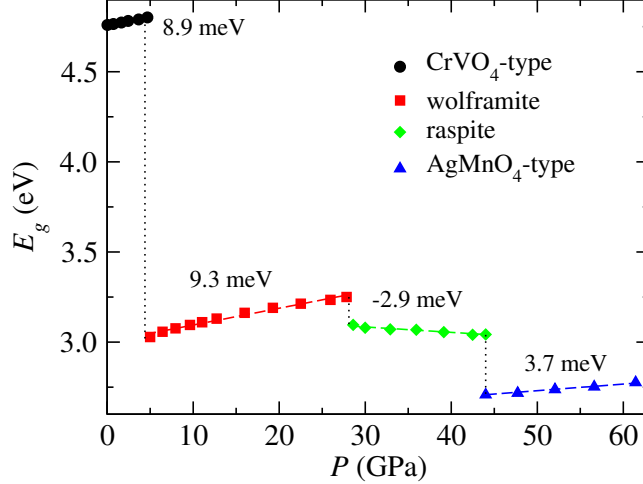


Figure 10: (Color online) Pressure evolution of gap energy of  $\text{InVO}_4$ .

hybrid functional. The details about the optimization of the crystal structure with this functional are described in Section 2. Figure 9 shows the band structure and the partial density of states for (a) the  $\text{CrVO}_4$ -type, (b) wolframite, (c) raspite, and (d)  $\text{AgMnO}_4$ -type phases at the respective pressure. Whereas Fig. 10 shows the pressure evolution of the energy band gap of  $\text{InVO}_4$ .

According to our calculations of band structure, Fig. 9 (a), the phase III of  $\text{InVO}_4$  is a direct band-gap material (top of valence band at Y and bottom of conduction band at Y). Where the top of the valence band consists mainly of O  $2p$  states. The bottom of the conduction band is dominated by V  $3d$  states with a not negligible contribution of O  $2p$  and In  $5s$  states. Similar results were obtained in Refs. 29 and 84. For this phase a direct electronic band-gap of 4.76 eV was obtained. On the other hand, we found that  $\text{InVO}_4$ -III presents an indirect electronic band-gap (top of valence band at  $\Gamma$  and bottom of conduction band at Y) of 3.06 eV when the AM05 functional is used.

As pressure is applied the band-gap in the  $\text{CrVO}_4$ -type phase increases with a pressure coefficient of 8.9 meV/GPa, as seen on Fig. 10. At this point we have to mention that there are important differences with the results obtained with AM05 functional. Where, we observed that as pressure increases the material changes from an indirect to a direct band-gap

at Y point with a pressure coefficient of -4.2 eV.

At the phase transition from CrVO<sub>4</sub>-type structure to wolframite we observed a collapse of the band gap which becomes close to 1.77 eV. In this phase we observed that the top of the valence band and the bottom of conduction band are located at Z point. Again, the orbital contribution to the top of the valence band and the bottom of the conduction band is similar than in the low-pressure phase but the conduction band are also populated with small contributions from O 2s and In 5p. The band gap collapse is consistent with the observation made in the study performed by Errandonea *et al.* in Ref. 25. On the other hand, the theoretical results from Ref. 29 show that wolframite phase is an indirect band-gap material with the top of the valence band at  $\Gamma$  and the bottom of the conduction band at Z. Our findings show that, as in the band-gap behavior of CrVO<sub>4</sub>-type structure under pressure, the band gap of wolframite increases with pressure with a pressure coefficient of 9.3 meV/GPa. Almost the same value was obtained with the AM05 functional. Similar values were observed in the high pressure studies of some wolframates such as MgWO<sub>4</sub>, ZnWO<sub>4</sub> and CdWO<sub>4</sub>.<sup>60</sup>

As seen on Fig. 9 (c) raspite phase has a direct band-gap at  $\Gamma$  point. While AgMnO<sub>4</sub>-type behave like a indirect band-gap material with the top of the valence band at  $\Gamma$  and the bottom of the conduction band at Z point, Fig. 9 (d) . In these phases the top of the valence band is almost all populated by O 2p states, whereas the bottom of the conduction band is mainly occupied by V 3d states. In these phases are produced additional reductions of the band-gap value, becoming the band-gap of AgMnO<sub>4</sub>-type phase 2.8 (1.2) eV at 60 GPa with the HSE06 (AM05) functional. Consequently, the band gap of InVO<sub>4</sub> changes from 4.76 (3.06) eV at ambient pressure to 2.8 (1.2) eV at 60 GPa with the hybrid HSE06 (AM05) functional. Such a large change of the electronic band gap has been observed in PbCrO<sub>4</sub> for ABO<sub>4</sub> oxides.<sup>86</sup>

In this study we observe significative differences when the electronic structure is calculated with the GGA AM05 and the hybrid HSE06 exchange correlation functional, being

the most significant differences on the electronic band-gap values, the determination if the band-gap is direct or indirect, and the slope of the band-gap pressure coefficients. Unfortunately, there are no compelling experimental studies in the literature to support or disprove our findings. We hope that this work will serve to encourage the experimental scientists to study the electronic structure of  $\text{InVO}_4$  at ambient conditions and under pressure.

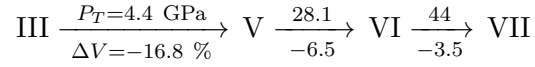
## 4 Summary and Conclusions

We presented a first principles study of structural, electronic and vibrational properties of  $\text{InVO}_4$  from ambient pressure to 62 GPa. The quasi-harmonic approximation has been used to obtain the Gibbs free energy and determine the phase transitions at ambient temperature. Where a good agreement between our theoretical results and the reported experimental data was obtained. In our study we found that wolframite presents a drastic change in the interatomic bond distances in order to increase the coordination of In at elevated pressures, which has an important effect in the Raman and infrared phonon frequencies at  $\Gamma$  point, but also in the branches of the phonon spectrum in other points of the Brillouin zone. It has been observed that the characteristic acoustic  $B_u$  infrared phonon mode of wolframite, the phonon mode that has negative pressure coefficient and Grüneisen parameter, softens completely around 14 GPa. Which is related with the instability of the wolframite phase as pressure increases. Besides, in our study two new high pressure phases were observed above 28 GPa, being the raspite and  $\text{AgMnO}_4$ -type structure. As is known the last one was observed as post-scheelite phase in  $\text{CaSeO}_4$  and as a high-pressure phase of  $\text{CaSO}_4$ .

It has been proposed that pressure could induce the metallization of orthovanadates at relative low pressure (11 GPa)<sup>87</sup> however our calculations show that  $\text{InVO}_4$  does not become metallic up to 60 GPa.

The information of transition pressure and volume reduction involved in the phase transition sequence observed in  $\text{InVO}_4$  in this study from phase III ( $\text{CrVO}_4$ -) to VII ( $\text{AgMnO}_4$ -type

structure) can be summarized as follows:



## Author Information

### Corresponding Author

\*E-mail: sinlopez@uacam.mx

### Author Contributions

The manuscript was written through contributions of all authors. All authors have given approval to the final version of the manuscript.

### Notes

The authors declare no competing financial interests.

## Acknowledgement

This work has been done under partial financial support from Spanish MINECO under projects MAT2013-46649-C4-1/3-P, MAT2015-71070-REDC, and MAT2016-75586-C4-1/3-P. S.M.L. thanks CONACYT from Mexico for financial support through the program "Cátedras para Jóvenes Investigadores". We thank the computer time provided by the RES (Red Española de Supercomputación) and the MALTA cluster.

## References

- (1) Errandonea, D.; Manjón, F. J. Pressure effects on the structural and electronic properties of  $ABX_4$  scintillating crystals. *Prog. Mater. Sci.* **2008**, *53*, 711–773.
- (2) Rapaport, A.; David, V.; Bass, M.; Deka, C.; Boatner, L. Optical spectroscopy of erbium-doped lutetium orthophosphate. *J. Luminescence* **1999**, *85*, 155–161.
- (3) Rapaport, A.; Moteau, O.; Bass, M.; Boatner, L. A.; Deka, C. Optical spectroscopy and lasing properties of neodymium-doped lutetium orthophosphate. *J. Opt. Soc. Am. B* **1999**, *16*, 911–916.
- (4) Lempicki, A.; Berman, E.; Wojtowicz, A.; Balcerzyk, M.; Boatner, L. Cerium-doped orthophosphates: new promising scintillators. *Nuclear Science, IEEE Transactions on* **1993**, *40*, 384–387.
- (5) Allison, S. W.; Boatner, L. A.; Gillies, G. T. Characterization of high-temperature thermographic phosphors: spectral properties of  $\text{LuPO}_4:\text{Dy}(1\%),\text{Eu}(2\%)$ . *Appl. Opt.* **1995**, *34*, 5624–5627.
- (6) Baran, E. J. Materials belonging to the  $\text{CrVO}_4$  structure type: preparation, crystal chemistry and physicochemical properties. *J. Mater. Sci.* **1998**, *33*, 2479–2497.
- (7) Ai, Z.; Zhang, L.; Lee, S. Efficient Visible Light Photocatalytic Oxidation of NO on Aerosol Flow-Synthesized Nanocrystalline  $\text{InVO}_4$  Hollow Microspheres. *J. Phys. Chem. C* **2010**, *114*, 18594–18600.
- (8) Lin, H.-Y.; Chen, Y.-F.; Chen, Y.-W. Water splitting reaction on  $\text{NiO}/\text{InVO}_4$  under visible light irradiation. *Inter. J. Hydrogen Energy* **2007**, *32*, 86–92.
- (9) Dennis P. Butcher, J.; Gewirth, A. A. Photoelectrochemical Response of  $\text{TlVO}_4$  and  $\text{InVO}_4$ :  $\text{TlVO}_4$  Composite. *Chem. Mater.* **2010**, *22*, 2555–2562.

- (10) Zou, Z.; Ye, J.; Sayama, K.; Arakawa, H. Direct splitting of water under visible light irradiation with an oxide semiconductor photocatalyst. *Nature* **2001**, *414*, 625–627.
- (11) Panchal, V.; López-Moreno, S.; Santamaría-Pérez, D.; Errandonea, D.; Manjón, F. J.; Rodríguez-Hernandez, P.; Muñoz, A.; Achary, S. N.; Tyagi, A. K. Zircon to monazite phase transition in  $\text{CeVO}_4$ : X-ray diffraction and Raman-scattering measurements. *Phys. Rev. B* **2011**, *84*, 024111.
- (12) Errandonea, D.; Lacomba-Perales, R.; Ruiz-Fuertes, J.; Segura, A.; Achary, S. N.; Tyagi, A. K. High-pressure structural investigation of several zircon-type orthovanadates. *Phys. Rev. B* **2009**, *79*, 184104.
- (13) Tomeno, I.; Sato, N.; Sato, Y.; Oka, K.; Tsunoda, Y. Neutron scattering study of acoustic phonon softening in  $\text{BiVO}_4$ . *Phys. Rev. B* **2011**, *84*, 014302.
- (14) Clavier, N.; Podor, R.; Dacheux, N. Crystal chemistry of the monazite structure. *J. European Ceramic Soc.* **2011**, *31*, 941–976.
- (15) Touboul, M.; Melghit, K. Synthesis by Chimie douce and properties of chromium (III) vanadates(V). *J. Mater. Chem.* **1995**, *5*, 147–150.
- (16) Tojo, T.; Zhang, Q.; Saito, F. Mechanochemical synthesis of rutile-type  $\text{CrMO}_4$  (M=V, Sb) and their solid solutions. *J. Solid State Chem.* **2006**, *179*, 433–437.
- (17) Oka, Y.; Yao, T.; Yamamoto, N.; Ueda, Y.; Kawasaki, S.; Azuma, M.; Takano, M. Hydrothermal Synthesis, Crystal Structure, and Magnetic Properties of  $\text{FeVO}_4$ -II. *J. Solid State Chem.* **1996**, *123*, 54–59.
- (18) Robertson, B.; Kostiner, E. Crystal structure and Mössbauer effect investigation of  $\text{FeVO}_4$ . *J. Solid State Chem.* **1972**, *4*, 29–37.

- (19) Muller, J.; Joubert, J. Synthèse sous haute pression d'oxygène d'une forme dense ordonnée de  $\text{FeVO}_4$  et mise en évidence d'une variété allotropique de structure  $\text{CrVO}_4$ . *J. Solid State Chem.* **1975**, *14*, 8–13.
- (20) Touboul, M.; Ingrain, D. Synthèses et propriétés thermiques de  $\text{InVO}_4$  et  $\text{TlVO}_4$ . *J. Less Common Metals* **1980**, *71*, 55–62.
- (21) Baran, E. J.; Escobar, M. E. The vibrational spectra of  $\text{InVO}_4$  and  $\text{TlVO}_4$ . *Spectrochimica Acta Part A: Molecular Spectroscopy* **1985**, *41*, 415–417.
- (22) Enache, C. S.; Lloyd, D.; Damen, M. R.; Schoonman, J.; van de Krol, R. Photoelectrochemical Properties of Thin-Film  $\text{InVO}_4$  Photoanodes: the Role of Deep Donor States. *J. Phys. Chem. C* **2009**, *113*, 19351–19360.
- (23) van de Krol, R.; Ségalini, J.; Enache, C. S. Influence of point defects on the performance of  $\text{InVO}_4$  photoanodes. *J. Photonics Energy* **2011**, *1*, 016001.
- (24) Katari, V.; Patwe, S. J.; Achary, S. N.; Tyagi, A. K. High Temperature Structural, Dielectric, and Ion Conduction Properties of Orthorhombic  $\text{InVO}_4$ . *J. Amer. Ceram. Soc.* **2013**, *96*, 166–173.
- (25) Errandonea, D.; Gomis, O.; García-Domene, B.; Pellicer-Porres, J.; Katari, V.; Achary, S. N.; Tyagi, A. K.; Popescu, C. New Polymorph of  $\text{InVO}_4$ : A High-Pressure Structure with Six-Coordinated Vanadium. *Inorg. Chem.* **2013**, *52*, 12790–12798.
- (26) Touboul, M.; Tolédano, P. Structure du vanadate d'indium:  $\text{InVO}_4$ . *Acta Cryst. B* **1980**, *36*, 240–245.
- (27) Roncaglia, D.; Botto, I.; Baran, E. Characterization of a low-temperature form of  $\text{InVO}_4$ . *J. Solid State Chem.* **1986**, *62*, 11–15.
- (28) Touboul, M.; Melghit, K.; Bénard, P.; Louër, D. Crystal Structure of a Metastable Form of Indium Orthovanadate,  $\text{InVO}_4$ -I. *J. Solid State Chem.* **1995**, *118*, 93–98.

- (29) Mondal, S.; Appalakondaiah, S.; Vaitheeswaran, G. High pressure structural, electronic, and optical properties of polymorphic  $\text{InVO}_4$  phases. *J. Appl. Phys.* **2016**, *119*, 085702.
- (30) Ruiz-Fuertes, J.; Errandonea, D.; López-Moreno, S.; González, J.; Gomis, O.; Vila-plana, R.; Manjón, F. J.; Muñoz, A.; Rodríguez-Hernández, P.; Friedrich, A.; Tupitsyna, I. A.; Nagornaya, L. L. High-pressure Raman spectroscopy and lattice-dynamics calculations on scintillating  $\text{MgWO}_4$ : Comparison with isomorphic compounds. *Phys. Rev. B* **2011**, *83*, 214112.
- (31) Grochala, W.; Hoffmann, R.; Feng, J.; Ashcroft, N. The Chemical Imagination at Work in Very Tight Places. *Angew. Chem. Int. Ed.* **2007**, *46*, 3620–3642.
- (32) Mujica, A.; Rubio, A.; Muñoz, A.; Needs, R. J. High-pressure phases of group-IV, III-V, and II-VI compounds. *Rev. Mod. Phys.* **2003**, *75*, 863–912.
- (33) López-Moreno, S.; Errandonea, D. *Ab initio* prediction of pressure-induced structural phase transitions of  $\text{CrVO}_4$ -type orthophosphates. *Phys. Rev. B* **2012**, *86*, 104112.
- (34) Wang, Y.; Cao, G. Synthesis and electrochemical properties of  $\text{InVO}_4$  nanotube arrays. *J. Mater. Chem.* **2007**, *17*, 894–899.
- (35) Liu, J.; Cao, G.; Yang, Z.; Wang, D.; Dubois, D.; Zhou, X.; Graff, G.; Pederson, L.; Zhang, J.-G. Oriented Nanostructures for Energy Conversion and Storage. *Chem. Sus. Chem.* **2008**, *1*, 676–697.
- (36) Yi, X.; Li, J.; Chen, Z.; Tok, A. Single-Crystalline  $\text{InVO}_4$  Nanotubes by Self-Template-Directed Fabrication. *J. Amer. Ceram. Soc.* **2010**, *93*, 596–600.
- (37) Song, L.; Liu, S.; Lu, Q.; Zhao, G. Fabrication and characterization of electrospun orthorhombic  $\text{InVO}_4$  nanofibers. *Appl. Surf. Sci.* **2012**, *258*, 3789–3794.
- (38) Blöchl, P. E. Projector augmented-wave method. *Phys. Rev. B* **1994**, *50*, 17953–17979.

- (39) Kresse, G.; Joubert, D. From ultrasoft pseudopotentials to the projector augmented-wave method. *Phys. Rev. B* **1999**, *59*, 1758–1775.
- (40) Kresse, G.; Hafner, J. *Ab initio* molecular dynamics for liquid metals. *Phys. Rev. B* **1993**, *47*, 558–561.
- (41) Kresse, G.; Hafner, J. *Ab initio* molecular-dynamics simulation of the liquid-metal-amorphous-semiconductor transition in germanium. *Phys. Rev. B* **1994**, *49*, 14251–14269.
- (42) Kresse, G.; Furthmüller, J. Efficiency of ab-initio total energy calculations for metals and semiconductors using a plane-wave basis set. *Comput. Mat. Sci.* **1996**, *6*, 15.
- (43) Kresse, G.; Furthmüller, J. Efficient iterative schemes for *ab initio* total-energy calculations using a plane-wave basis set. *Phys. Rev. B* **1996**, *54*, 11169–11186.
- (44) Armiento, R.; Mattsson, A. E. Functional designed to include surface effects in self-consistent density functional theory. *Phys. Rev. B* **2005**, *72*, 085108.
- (45) Mattsson, A. E.; Armiento, R. Implementing and testing the AM05 spin density functional. *Phys. Rev. B* **2009**, *79*, 155101.
- (46) Mattsson, A. E.; Armiento, R.; Paier, J.; Kresse, G.; Wills, J. M.; Mattsson, T. R. The AM05 density functional applied to solids. *J. Chem. Phys.* **2008**, *128*, 084714.
- (47) Monkhorst, H. J.; Pack, J. D. Special points for Brillouin-zone integrations. *Phys. Rev. B* **1976**, *13*, 5188–5192.
- (48) Parlinski, K. Computer Code PHONON. See: <http://wolf.ifj.edu.pl/phonon> (accessed February 02, 2017).
- (49) Baroni, S.; de Gironcoli, S.; Dal Corso, A.; Giannozzi, P. Phonons and related crystal properties from density-functional perturbation theory. *Rev. Mod. Phys.* **2001**, *73*, 515–562.

- (50) Cazorla, C.; Errandonea, D.; Sola, E. *Phys. Rev. B* **2009**, *80*, 064105.
- (51) Cazorla, C.; Boronat, J. First-principles modeling of quantum nuclear effects and atomic interactions in solid  $^4\text{He}$  at high pressure. *Phys. Rev. B* **2015**, *91*, 024103.
- (52) Heyd, J.; Scuseria, G. E.; Ernzerhof, M. Hybrid functionals based on a screened Coulomb potential. *J. Chem. Phys.* **2003**, *118*, 8207–8215.
- (53) Heyd, J.; Scuseria, G. E. Efficient hybrid density functional calculations in solids: Assessment of the Heyd-Scuseria-Ernzerhof screened Coulomb hybrid functional. *J. Chem. Phys.* **2004**, *121*, 1187–1192.
- (54) Heyd, J.; Scuseria, G. E.; Ernzerhof, M. Erratum: Hybrid functionals based on a screened Coulomb potential? [J. Chem. Phys. 118, 8207 (2003)]. *J. Chem. Phys.* **2006**, *124*, 219906.
- (55) Paier, J.; Marsman, M.; Hummer, K.; Kresse, G.; Gerber, I. C.; Ángyán, J. G. Screened hybrid density functionals applied to solids. *J. Chem. Phys.* **2006**, *124*, 154709.
- (56) Birch, F. Finite Elastic Strain of Cubic Crystals. *Phys. Rev.* **1947**, *71*, 809–824.
- (57) Abrahams, S. C.; Reddy, J. M. Crystal Structure of the Transition-Metal Molybdates. I. Paramagnetic  $\alpha\text{-MnMoO}_4$ . *J. Chem. Phys.* **1965**, *43*, 2533–2543.
- (58) Sleight, A. W.; Chamberland, B. L. Transition metal molybdates of the type  $\text{AMoO}_4$ . *Inorg. Chem.* **1968**, *7*, 1672–1675.
- (59) Ruiz-Fuertes, J.; López-Moreno, S.; Errandonea, D.; Pellicer-Porres, J.; Lacomba-Perales, R.; Segura, A.; Rodríguez-Hernández, P.; Muñoz, A.; Romero, A. H.; González, J. High-pressure phase transitions and compressibility of wolframite-type tungstates. *J. Appl. Phys.* **2010**, *107*, 083506.

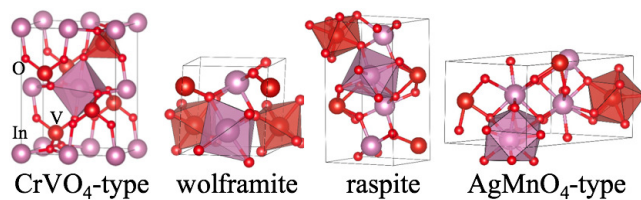
- (60) Ruiz-Fuertes, J.; López-Moreno, S.; López-Solano, J.; Errandonea, D.; Segura, A.; Lacomba-Perales, R.; Muñoz, A.; Radescu, S.; Rodríguez-Hernández, P.; Gospodinov, M.; Nagornaya, L. L.; Tu, C. Y. Pressure effects on the electronic and optical properties of  $AWO_4$  wolframites ( $A = \text{Cd, Mg, Mn, and Zn}$ ): The distinctive behavior of multiferroic  $\text{MnWO}_4$ . *Phys. Rev. B* **2012**, *86*, 125202.
- (61) López-Moreno, S.; Romero, A. H.; Rodríguez-Hernández, P.; Muñoz, A. Ab initio calculations of the wolframite  $\text{MnWO}_4$  under high pressure. *High Press. Res.* **2009**, *29*, 578–581.
- (62) Sleight, A. W. Accurate cell dimensions for  $ABO_4$  molybdates and tungstates. *Acta Cryst. B* **1972**, *28*, 2899–2902.
- (63) Ruiz-Fuertes, J.; Errandonea, D.; Lacomba-Perales, R.; Segura, A.; González, J.; Rodríguez, F.; Manjón, F. J.; Ray, S.; Rodríguez-Hernández, P.; Muñoz, A.; Zhu, Z.; Tu, C. Y. High-pressure structural phase transitions in  $\text{CuWO}_4$ . *Phys. Rev. B* **2010**, *81*, 224115.
- (64) Gracia, L.; Beltrán, A.; Errandonea, D. Characterization of the  $\text{TiSiO}_4$  structure and its pressure-induced phase transformations: Density functional theory study. *Phys. Rev. B* **2009**, *80*, 094105.
- (65) Gracia, L.; Beltrán, A.; Errandonea, D.; Andrés, J.  $\text{CaSO}_4$  and Its Pressure-Induced Phase Transitions. A Density Functional Theory Study. *Inorg. Chem.* **2012**, *51*, 1751–1759.
- (66) López-Moreno, S.; Errandonea, D.; Rodríguez-Hernández, P.; Muñoz, A. Polymorphs of  $\text{CaSeO}_4$  under Pressure: A First-Principles Study of Structural, Electronic, and Vibrational Properties. *Inorg. Chem.* **2015**, *54*, 1765–1777.
- (67) Young, A. P.; Schwartz, C. M. High pressure forms of  $\text{CrVO}_4$  and  $\text{FeVO}_4$ . *Acta Cryst.* **1962**, *15*, 1305.

- (68) Laves, F.; Young, A. P.; Schwartz, C. M. On the high-pressure form of  $\text{FeVO}_4$ . *Acta Cryst.* **1964**, *17*, 1476–1477.
- (69) Garg, A. B.; Errandonea, D.; Rodríguez-Hernández, P.; López-Moreno, S.; Muñoz, A.; Popescu, C. High-pressure structural behaviour of  $\text{HoVO}_4$ : combined XRD experiments and *ab initio* calculations. *J. Phys.: Condens. Matter* **2014**, *26*, 265402.
- (70) López-Moreno, S.; Rodríguez-Hernández, P.; Muñoz, A.; Romero, A. H.; Errandonea, D. First-principles calculations of electronic, vibrational, and structural properties of scheelite  $\text{EuWO}_4$  under pressure. *Phys. Rev. B* **2011**, *84*, 064108.
- (71) Panchal, V.; Errandonea, D.; Segura, A.; Rodríguez-Hernández, P.; Muñoz, A.; López-Moreno, S.; Bettinelli, M. The electronic structure of zircon-type orthovanadates: Effects of high-pressure and cation substitution. *J. Appl. Phys.* **2011**, *110*, 043723.
- (72) Errandonea, D.; Achary, S. N.; Pellicer-Porres, J.; Tyagi, A. K. Pressure-Induced Transformations in  $\text{PrVO}_4$  and  $\text{SmVO}_4$  and Isolation of High-Pressure Metastable Phases. *Inorg. Chem.* **2013**, *52*, 5464–5469.
- (73) Crichton, W. A.; Parise, J. B.; Antao, S. M.; Grzechnik, A. Evidence for monazite-, barite-, and  $\text{AgMnO}_4$  (distorted barite)-type structures of  $\text{CaSO}_4$  at high pressure and temperature. *Mineral. Mag.* **2005**, *90*, 22–27.
- (74) Gleissner, J.; Errandonea, D.; Segura, A.; Pellicer-Porres, J.; Hakeem, M. A.; Proctor, J. E.; Raju, S. V.; Kumar, R. S.; Rodríguez-Hernández, P.; Muñoz, A.; Lopez-Moreno, S.; Bettinelli, M. Monazite-type  $\text{SrCrO}_4$  under compression. *Phys. Rev. B* **2016**, *94*, 134108.
- (75) Panchal, V.; Manjón, F. J.; Errandonea, D.; Rodríguez-Hernández, P.; López-Solano, J.; Muñoz, A.; Achary, S. N.; Tyagi, A. K. High-pressure study of  $\text{ScVO}_4$  by Raman scattering and *ab initio* calculations. *Phys. Rev. B* **83**, 064111.

- (76) Errandonea, D.; Manjón, F.; Muñoz, A.; Rodríguez-Hernández, P.; Panchal, V.; Achary, S.; Tyagi, A. High-pressure polymorphs of  $\text{TbVO}_4$ : A Raman and ab initio study. *J. Alloys Compounds* **2013**, *577*, 327 – 335.
- (77) Errandonea, D.; Popescu, C.; Garg, A. B.; Botella, P.; Martínez-García, D.; Pellicer-Porres, J.; Rodríguez-Hernández, P.; Muñoz, A.; Cuenca-Gotor, V.; Sans, J. A. Pressure-induced phase transition and band-gap collapse in the wide-band-gap semiconductor  $\text{InTaO}_4$ . *Phys. Rev. B* **2016**, *93*, 035204.
- (78) Lacomba-Perales, R.; Errandonea, D.; Segura, A.; Ruiz-Fuertes, J.; Rodríguez-Hernández, P.; Radescu, S.; Lopez-Solano, J.; Mujica, A.; Muñoz, A. A combined high-pressure experimental and theoretical study of the electronic band-structure of scheelite-type  $\text{AWO}_4$  (A=?Ca, Sr, Ba, Pb) compounds. *J. Appl. Phys.* **2011**, *110*, 043703.
- (79) Paszkowicz, W.; Lopez-Solano, J.; Piszora, P.; Bojanowski, B.; Mujica, A.; Muñoz, A.; Cerenius, Y.; Carlson, S.; Dabkowska, H. Equation of state and electronic properties of  $\text{EuVO}_4$ : A high-pressure experimental and computational study. *J. Alloys Comp.* **2015**, *648*, 1005–1016.
- (80) Zurek, E.; Grochala, W. Predicting crystal structures and properties of matter under extreme conditions via quantum mechanics: the pressure is on. *Phys. Chem. Chem. Phys.* **2015**, *17*, 2917–2934.
- (81) López, S.; Romero, A. H.; Mejía-López, J.; Mazo-Zuluaga, J.; Restrepo, J. Structure and electronic properties of iron oxide clusters: A first-principles study. *Phys. Rev. B* **2009**, *80*, 085107.
- (82) Shishkin, M.; Kresse, G. Self-consistent *GW* calculations for semiconductors and insulators. *Phys. Rev. B* **2007**, *75*, 235102.

- (83) Hermann, A.; Derzsi, M.; Grochala, W.; Hoffmann, R. AuO: Evolving from Dis- to Comproportionation and Back Again. *Inorg. Chem.* **2016**, *55*, 1278–1286.
- (84) Li, G.-L.; Yin, Z. Theoretical insight into the electronic, optical and photocatalytic properties of InMO<sub>4</sub> (M = V, Nb, Ta) photocatalysts. *Phys. Chem. Chem. Phys.* **2011**, *13*, 2824–2833.
- (85) He, T.; Ehrhart, P.; Meuffels, P. Optical band gap and Urbach tail in Y<sup>3+</sup>-doped BaCeO<sub>3</sub>. *J. Appl. Phys.* **1996**, *79*, 3219–3223.
- (86) Errandonea, D.; Bandiello, E.; Segura, A.; Hamlin, J.; Maple, M.; Rodriguez-Hernandez, P.; Noz, A. M. Tuning the band gap of PbCrO<sub>4</sub> through high-pressure: Evidence of wide-to-narrow semiconductor transitions. *J. Alloys Comp.* **2014**, *587*, 14–20.
- (87) Garg, A. B.; Shanavas, K.; Wani, B.; Sharma, S. M. Phase transition and possible metallization in CeVO<sub>4</sub> under pressure. *J. Solid State Chem.* **2013**, *203*, 273–280.

## Graphical TOC Entry



InVO<sub>4</sub> under pressure

The high-pressure stability of InVO<sub>4</sub> is investigated using *ab initio* calculations. Where the phase transitions driven by pressure were determined within the quasiharmonic approximation at 300 K. In our findings two new HP post-wolframite phases were obtained. The equation of state, crystal structure, phonon spectrum and electronic structure were studied for each stable phase as well as their evolution with pressure.

**For Table of Contents Only**